

HST Observations of the Main Sequence of M4¹

H.B. Richer, G.G. Fahlman², J. Brewer, S. Davis, J. Kalirai

Dept. of Physics and Astronomy, University of British Columbia

richer/jbrewer/jkalirai@astro.ubc.ca

greg.fahlman@nrc-cnrc.gc.ca

P.B. Stetson

National Research Council, Herzberg Institute of Astrophysics

peter.stetson@nrc-cnrc.gc.ca

B.M.S. Hansen, R.M. Rich

Department of Physics and Astronomy, University of California at Los Angeles

hansen/rmr@astro.ucla.edu

R.A. Ibata

Observatoire de Strasbourg

ibata@newb6.u-strasbg.fr

B. K. Gibson

Centre for Astrophysics and Supercomputing, Swinburne University

bgibson@astro.swin.edu.au

M. Shara

American Museum of Natural History

mshara@amnh.org

ABSTRACT

This paper presents new results from a photometric study of the main-sequence stars in M4 (NGC 6121 = GC 1620–264), the closest globular cluster to the sun. Multi-field, multi-epoch observations at approximately 1, 2, and 6 core-radii were obtained with the WFPC2 camera on the HST through either *F606W* or *F555W* (*V*) and *F814W* (*I*) filters. The multi-epoch observations allowed us to clean the data on the basis of proper motion and thus separate cluster from field stars or extragalactic objects. In all the fields the cluster main sequence can be traced to at least $V = 27.0$ but there remains a trail of stars to the limit of the data near $V = 30$ in the deepest outer

¹Based on observations with the NASA/ESA Hubble Space Telescope, obtained at the Space Telescope Science Institute, which is operated by AURA under NASA contract NAS 5-26555. These observations are associated with proposals GO-5461 and GO-8679.

²Herzberg Institute of Astrophysics

field. There is no evidence that we have reached the end of the hydrogen burning main sequence in any of our fields, however, there is some indication that very few stars remain to be detected in the deepest data.

A study of the scatter about the cluster main sequence yields a surprisingly small and variable binary fraction; $f_b \simeq 2\%$ in the inner parts of the cluster falling to the 1% range outside. However, with one possible exception, no stars in the 6 core radius field exhibit photometric variability on timescales of a few hours through a few days. For the currently visible main sequence stars, the cluster mass function is very flat ($\alpha = 0.1$) in the outer field and flattens further in the inner fields suggesting well developed mass segregation. The observed variation in the mass function is broadly consistent with isotropic, multi-mass Michie-King models. Because we have a large sample of white dwarfs in the outer field we are able to show that the cluster IMF above $0.8M_\odot$ was considerably steeper than the present day mass function for low mass stars.

Two appendices are included in this contribution. The first one is a detailed discussion of the techniques used to reduce the data while the second provides a direct comparison between the cluster stars and those belonging to the inner spheroid of the Galaxy. This yields a relative distance between the cluster, d_c , and the Galactic center, R_o , of $R_o/d_c = 4.36 \pm 0.13$. With our subdwarf-based estimate of $d_c = 1.73 \pm 0.09$ kpc to M4, we find $R_o = 7.5 \pm 0.6$ kpc.

Subject headings: globular clusters, clusters individual: M4

1. Introduction

The high angular resolution achievable with the Hubble Space Telescope offers at least four significant advantages over ground based observations of globular star clusters: (1) decreased blending makes accurate photometry to faint levels feasible in crowded cluster cores, (2) the improved contrast of the sharper stellar profile against a lower background allows photometry of very faint stars, (3) the sharp stellar profile makes possible the measurement of proper motions on short time baselines which facilitates separation of cluster and field objects, and (4) image morphology can be more effectively used to exclude extragalactic objects. By exploiting all of these improvements, we have been able to study two stellar populations, the cluster white dwarfs and the low-mass main-sequence stars, which have proven inaccessible from the ground (Richer et al. 1995, 1997, 2002; Hansen et al. 2002). These stars play key roles in the dynamical evolution of the clusters and provide important data pertaining to the theory of stellar evolution and star formation in the early universe. In this paper, we will present the results of our study of the main sequence stars of Messier 4 (NGC 6121 = C1620-264) derived from multi-field and multi-epoch HST observations under our cycles 4 and 9 proposals (GO-5461, GO-8679) as well as second epoch archival observations obtained from GO-8153.

The properties of M4 relevant to this study are summarized in Table 1. A critical review of earlier work on the reddening, distance modulus and metallicity of M4 is given by Dixon & Longmore 1993. Here, we adopt a distance modulus of $(m - M)_V = 12.51 \pm 0.09$ and a reddening a $E(V - I) = 0.51 \pm 0.02$, which were derived by fitting the subdwarfs listed in Mandushev et al. 1996 to the cluster main sequence as discussed in Richer et al. 1997.¹

For the preferred value of the ratio $R_V = A_V/E(B - V) = 3.8$ (Richer et al. 1997 and references therein), these estimates imply a physical distance to M4 of 1.73 kpc, which is in excellent agreement with the astrometric value of 1.72 ± 0.14 kpc (Peterson et al. 1995) and with the earlier distance based on a Baade-Wesselink analysis of four cluster RR Lyrae variables (Liu & Janes 1990). M4 is the globular cluster nearest to the Sun. There is

¹These quantities are for magnitudes defined in the Johnson-Cousins system. In the current paper all magnitudes are in the natural HST system so that these quantities are slightly different. See Table 1 for the extinctions used in this photometric system.

evidence for variable reddening across the entire M4 field (Cudworth & Rees 1990), (Lyons et al. 1995). Some differential reddening was seen in a field which overlaps part of our HST data (Fahlman et al. (1996b)), but there are no obvious effects which may be attributed to differential reddening in our photometric data.

The iron abundance quoted in Table 1 is from the spectroscopic analysis of four giants by Drake et al. (1994). The metallicity value preferred by Dixon & Longmore (1993), $[\text{Fe}/\text{H}] = -1.1 \pm 0.25$, is in good agreement with this value, as is the mean of all the previous work cited by Drake et al. (1994), $[\text{Fe}/\text{H}] = -1.17 \pm 0.31$. Carney (1996), who lists $[\text{Fe}/\text{H}] = -1.18$ for this cluster has reviewed the existing data on the α -element enhancement in M4, and derived a value of $[\alpha/\text{Fe}] = 0.30$. Subsequent to Carney’s review, Carretta & Gratton (1997) found $[\text{Fe}/\text{H}] = -1.19 \pm 0.03$ for M4 from three giants. Also Routledge et al. (1997) used new Ca triplet measurements for 17 M4 giants as part of a reanalysis of the globular cluster metallicity scale, and report $[\text{Fe}/\text{H}] = -1.27 \pm 0.04$ on the Zinn-West scale, and $[\text{Fe}/\text{H}] = -1.05 \pm 0.03$ on the Carretta-Gratton scale. Clearly, the specification of cluster metallicities accurate to the precision of individual studies continues to be a challenge. The space velocity of M4 has been measured recently by Bedin et al. (2003) and Kalirai et al. (2003) and the cluster appears to have a chaotic orbit confined closely to the disk, but avoiding the inner ~ 1 kpc of the Galaxy (Dauphole et al. 1996). Consequently, the dynamical evolution of the stellar population in M4 has probably been strongly affected by tidal interactions with the Galactic disk.

The dynamical parameters listed in Table 1 are based on the multi-mass Michie-King (MMK) models described in §7 of this paper. The derived scale radius differs only slightly from that of Trager et al. (1993), $r_s = 55''$. The concentration parameter, $c = \log(r_t/r_c) = 1.75$, where r_t is the (model) tidal radius and r_c refers to the conventional core radius of the luminous stars in M4. This is larger than the Trager et al. (1993) value, $c = 1.55$, but this is entirely due to the extended tidal radius of our MMK model. The half-mass relaxation time, t_{rh} , was calculated using the Spitzer formula as in Trager et al. (1993) but with a mean stellar mass and half-mass radius, $r_h = 6.67 r_s$, taken from our multi-mass King model. The central relaxation time, t_{rc} , was similarly obtained. To calculate these numbers, we need to estimate the cluster mass, and the mass to light ratios at the cluster center, $(\mathcal{M}/\mathcal{L})_0$, as well as the global value, \mathcal{M}/\mathcal{L} . For this purpose, we have used the the observed central velocity dispersion, $v_0 = 4.2 \text{ km s}^{-1}$ taken from Pryor and Meylan (1993). The values listed in Table 1 differ from those in the Pryor and Meylan (1993) compilation only because we have applied our distance modulus and extinction values to the same photometry that they used, and, of course, are using our MMK model for the relevant calculated quantities.

The small values of t_{rh} and t_{rc} compared to the nominal cluster age of $T = 12.7 \text{ Gyr}$ (see Hansen et al. 2002) strongly suggests that the stellar population in M4 is well relaxed. Indeed the ratio T/t_{rh} is so high that M4 is expected to have experienced a core collapse (Cohn 1980, Murphy & Cohn 1988) for which there is no evidence. Therefore, like the structurally similar cluster M71, studied in detail by Drukier et al. (1992), M4 is expected to have an internal energy source capable of preventing core collapse. Primordial binary stars are a good candidate for this energy source (Côté & Fischer 1996), and this provides strong motivation for examining the cluster binary frequency.

M4 has been the subject of a number of previous photometric studies. Richer & Fahlman (1984) obtained the first color-magnitude diagram with a CCD detector and notable subsequent studies are those of Alcaïno et al. (1988), Kanatas et al. (1995), Richer et al. (1995, 1997), Alcaïno et al. (1997), Pulone et al. (1999), Bedin et al. (2001), Richer et al. (2002,) and Hansen et al. (2002).

The scope of this paper is as follows. Following a detailed account of the data reduction in §2 and the first appendix, we describe the general properties of the cluster color-magnitude diagram in §3. In §4, we review the observational evidence for a photometric binary sequence. The cluster main sequence luminosity and mass functions are derived in §5. In §6 we address the question whether we have reached the end of the hydrogen-burning main sequence in M4. In §7 we interpret the observed mass-segregation with static MMK models and this, with input from the current state of dynamical modelling for globular star clusters in general, allows us to provide an estimate the cluster IMF. The final section provides an overview of the paper and discusses the

major results. A second appendix discusses the spheroid main sequence seen projected behind M4 and here we estimate the ratio of the distance to M4 to the distance to the Galactic center. Since the M4 distance is well known this allows us to derive an accurate distance to the Galactic center.

2. Observations, Data Reduction & Reduced Photometry

All observations were obtained with the WFPC2 instrument on HST. Three fields were observed: (a) a field within one core radius of the cluster center, (2) a field at about $2 r_c$ and (3) an outer field at about $6 r_c$. A schematic map of the cluster showing the position of the three fields and its division into 4 annuli is given in Richer et al. (1997 see also Ibata et al. (1999)). Table 2 contains the geometry for each annulus. In GO-5461 data were obtained through the $F555W$ (V) and $F814W$ (I) filters in all fields. In GO-8679 very deep images were secured in both $F606W$ and $F814W$ in the 6 core radius field only and these served as the second epoch for the outer field. In the current paper the $F606W$ images are employed for proper motions only and are not used for any detailed analysis; for these we used the earlier $F555W$ images for uniformity with the other fields. We retrieved images in all 3 fields from the HST archives for GO-8153. These were restricted to $F814W$ exposures and were the second epoch images for the inner 2 fields. A summary of the exposures used in this paper is given in Table 3. The inner two fields were also observed through the $F336W$ (U) filter in order to separate better the white dwarfs from other stars. Those data were presented in Richer et al. (1995, 1997) and are rediscussed only briefly here as they have now been cleaned on the basis of proper motion.

With the data from GO-8679, we quickly discovered that the background was variable with time (see Figure 1) decreasing as the two months of data collection progressed. On the frames taken early on in the data collection we found that the background sky was almost a factor of 2 higher than expected. This was due to zodiacal light as M4 has an ecliptic latitude of $\sim 6^\circ$ and in late January the angle between the Sun and M4 only amounted to slightly more than 60° . As time progressed during the 67 days over which these outer field data were secured the Sun angle increased and the situation improved. The net effect of the higher background was to reduce our limiting magnitude by about 0.2 mags.

Our aim in reducing the M4 data sets was to produce the best and deepest photometry possible with the existing data set and to ascertain whether an individual star was a cluster member based on how it moved over a given temporal baseline. We achieved this by using cluster stars to register the frames, and then combined the frames from the 2 different epochs separately. As the frames were registered using the cluster stars, we expect that cluster stars (aside from internal motions of ~ 0.5 mas/year which is smaller than our measurement error) will appear to remain stationary, whereas non-cluster stars and extragalactic objects will appear to move on account of the differential motion between the cluster and the background (which consists mainly of stars in the inner halo of the Galaxy). This is graphically illustrated in Figure 2.

The raw data frames had the standard HST pipeline processing applied to them and a few additional corrections were also applied, as discussed in Richer et al. (1997, 2002). The photometry was carried out with the DAOPHOT/ALLSTAR package developed by Stetson (1994) with a quadratically varying point-spread function. As well the ALLFRAME (Stetson 1994) photometry program, standard IRAF routines, and some utility programs written in C and C-shell scripts for book-keeping purposes were also employed.

To the best of our knowledge, this is the first time that DAOPHOT has been used to make proper motion measurements on WFPC data. Further, since the processing was slightly non-standard, we have outlined our reduction procedures in some detail in the first appendix.

In the following Tables (4 - 7) we present our photometry from the M4 fields arranged by annuli. The calibration of the data follows the methodology described by Holzman et al. (1995). By applying the synthetic transformations detailed in Table 10 of that work, we placed the data on the natural system of HST, that is into $F555W$ and $F814W$ magnitudes. The column headings are RA , DEC (both J2000), $F555W$, $F814W$,

$\mu_\alpha \cos(\delta)$, μ_δ , where the latter 2 quantities are the proper motion displacements in RA and DEC in mas/yr measured with respect to an extragalactic reference frame (Kalirai et al. 2003).

3. The Color-Magnitude Diagram

The color-magnitude diagrams (CMDs) for stars selected to possess total proper motions appropriate to the cluster (within 5 mas/yr of that of the mean cluster motion) are shown in the ($F555W$, $F555W - F814W$) plane (hereafter referred to as $V, V - I$) in the left hand panels of Figures 3a-d. In these diagrams the stars are plotted in the 4 annuli defined in Richer et al. 1997. The mean cluster fiducial over the range $21 < V < 27$ for stars in the inner two annuli is listed in Table 8. At the upper end of this range saturation effects are just avoided (except in the outer field where they set in near $F555W = 22$) and at the faint end the main sequence fiducial ceases to be well defined because of a paucity of stars. The dispersion in the magnitude differences for stars of known magnitude inserted into the frames in both I and V are shown in Fig. 4 for stars in annulus 2. This is a reasonable representation of the errors for the rather short exposures used in the inner fields.

The most prominent feature along the main-sequence, the abrupt drop in star numbers at $V \simeq 27.0$, is *not* an artifact. A similar, but less dramatic, feature is apparent in the CMD of the metal-poor globular cluster NGC 6397 (King et al. 1998). This plunging luminosity function is likely accentuated by mass segregation (see §7) and occurs where the theoretical models (eg those of Montalbán et al. 2000) exhibit a change in the slope of the mass-luminosity relation. At brighter magnitudes, the CMD appears to broaden again but this effect arises predominantly from saturated stellar images ($V \leq 20.5$), which lead to large errors in the photometry. The individual CMDs show very clearly that the photometric completeness limit is a strong function of radius. The 6 r_c field is entirely contained in annulus 4 and is clearly the deepest data partly by design (the exposure time through the $F555W$ and $F814W$ filters was considerably longer than in the other fields) and partly because scattered light and bright star diffraction spikes are much less of a limiting factor compared to the inner fields.

4. Photometric Binaries

One unusual characteristic of M4 is that the central two-body relaxation time (see Table 1) is much smaller than the apparent age of the cluster and therefore the cluster core is expected to be in a state of core collapse. However, M4 does not exhibit a collapsed core and, therefore, as noted by [Côté & Fischer (1996), it may well have a centrally concentrated binary population because such stars are the most plausible source for the energy needed to prevent core collapse. Additional discussion of the M4 binary fraction in our data is given by Pryor et al. (1996), Richer et al. (1996a) and Ferdman et al. (2003).

A casual inspection of the CMDs of Fig. 3 suggests the possible presence of a few similar-mass photometric binaries located ≈ 0.75 magnitudes above the cluster main sequence. A better look at this can be obtained by inspecting the CMDs with a fiducial line included shifted by $\Delta V = -0.75$. Such a diagram is shown in Fig. 5 for each of the separate fields. Comparing the number of stars near this line for $V > 20$ (to avoid saturation effects) with the total number of main sequence stars suggests that no more than about 2% of the measured stars are approximately equal-mass binaries (see also Richer et al. 1996a). The actual measured percentages are 2.2, 1.1, 1.1 and 1.8% from inner to outer annuli (see Table 9). These must be considered upper limits as optical binaries are not included in this estimate. Almost identical percentages were estimated from an examination of the $U, U - I$ color magnitude diagrams in the inner fields. These colors are actually somewhat superior given their larger color baseline. This very low binary frequency is consistent with the apparent lack of variable stars in the outer annulus of our data (Ferdman et al. 2003).

As a consistency check on these conclusions we display in Figure 6 the results of a simulation of binaries

in our fields. The models of Montalban et al., the error distributions shown in Figure 4 and mass functions with slopes $\alpha = 0$ and 1 (see §5) were used to generate the CMDs shown here. The binaries were chosen at random from the mass function, random errors applied consistent with those in Figure 4 and, for comparison, a fiducial sequence 0.75 mags brighter than the main sequence is also included. It is clear from this diagram that binary frequencies in the range 1 - 2% are about right for our M4 fields whereas a frequency as high as 5% is incompatible with the observed CMDs.

The distribution of the residual in magnitudes of all cluster stars from the fiducial main sequence for each annulus is given in Fig. 7. Here we take the entire deviation of a star from the main sequence to be caused by a deviation in V and plot the histogram of this residual for stars in the magnitude range $V = 20 - 26$. In this diagram negative residuals are main sequence binaries (the star is brighter than the main sequence fiducial for its color) while the only explanation for positive residuals (other than non-cluster members) is a white dwarf - main sequence binary. Inspection of Fig. 7 suggests that a small approximately equal-mass main sequence binary fraction (of order 2%) may be present in annuli 1 and 2, a smaller fraction (near 1%) in annulus 3 and annulus 4 exhibits no obvious photometric binaries although there is a non-Gaussian tail in the residual distribution on the main sequence binary side. Annulus 2 may exhibit some evidence for a small component of white dwarf - main sequence binaries.

The derived binary fractions for the inner fields ($\simeq 2\%$) is higher than that indicated elsewhere. This supports (albeit weakly) the hypothesis of an enhanced central binary fraction, but some caution is necessary since the photometry in the central field is also the most affected by the presence of diffraction spikes from bright stars and related crowded-field artifacts which degrade the photometry. These statistical results need to be verified with radial velocity measurements on the possible binaries.

Côté & Fischer (1996) estimated a binary fraction of $f_b \simeq 15\%$, after correcting for their detection efficiency, from two detections of radial velocity variations among 33 stars. Their stars were located in the radial distance range: $3'.2 \leq r \leq 16'$. The inner part of their field is roughly the same radial distance as our outer field where we derive an estimate of $f_b \leq 2\%$. This difference is somewhat puzzling, but, in view of the uncertainties in both studies, can not be usefully pursued without a great deal more observational effort.

5. The Luminosity and Mass Functions

The cluster luminosity function (LF) is obtained by simply counting the main sequence stars. This procedure is much improved using proper motion selection as accounting for the field star contamination is no longer the serious problem that it used to be. The luminosity function itself contains rather limited information and cannot be compared directly from one globular cluster to another because of metallicity effects. The quantity that can be compared is the cluster mass function (MF).

In this work, we have adopted the policy of making the least possible manipulation to the observational data themselves and make all the needed corrections in the theoretical plane. This has the advantage that the errors in the observational quantities remain as purely statistical without introducing the problem of error propagation. For example, there are corrections for completeness effects in the star counting that must be applied and we have incorporated these with the theory.

Our method of proceeding is thus as follows. From the proper motion selected cluster main sequence we derive the luminosity function in each annulus. We then used the theoretical models of Montalban et al. (2000) and power-law mass functions to generate theoretical luminosity functions. These functions were then convolved with the detection efficiency in the data in order that they could be directly compared with the observations and normalized to contain the same number of stars as the observations. By this procedure then, there is no freedom to adjust the functions by arbitrary normalization. By a χ^2 process, the best fitting model luminosity function was chosen and the mass function slope for that luminosity function was then taken as the

appropriate mass function in that annulus.

The completeness of our data was determined with very extensive artificial star tests which were described briefly in Richer et al. 2002. The added stars were drawn from an M4 fiducial sequence and 4 trials of 1250 stars each were added into all the chips in all the fields. The stars were added onto a grid which insured that no artificial stars overlapped with each other. The position of the added star at the intersection points of this grid was given a small random offset to insure that stars were not all added at the same positions in the trials, but the shift was small compared with the grid and PSF size. This technique (first used by Piotto & Zoccali 1999) allows large numbers of stars to be added into a single frame while insuring that they do not interfere with each other (ie do not change the crowding statistics in the images). This guarantees that the corrections thus derived provide accurate incompleteness statistics. The incompleteness corrections applied were not a single number for a given magnitude, but we kept track of all the stars recovered irrespective at which magnitude they were recovered. From this we derived a “correction matrix” with input magnitude along one axis and recovered magnitude along the other. The diagonal elements of this matrix are the recovery fractions for stars recovered within the same magnitude bin as input while the off-diagonal ones are the recovery fractions for stars recovered either brighter or fainter than input. This matrix was then multiplied by the theoretical luminosity function for comparison with the observations. In this way the data remain untouched and all the corrections were done to the theoretical functions.

Another point to be made about deriving the MF is that the theoretical models used – those of Montalban et al. (2000) or any other models for that matter – for the theoretical mass-luminosity relation do not fit the lower main sequences of intermediate metallicity globular clusters very well. This is well illustrated in Bedin et al. (2001). At this point there is little that can be done about this other than to compare the MF slopes derived with the models available from several groups and to calculate the luminosity functions in both V and I independently and look for agreement in the derived MFs. We discuss these points more below.

Figures 8 and 9 illustrate the observed LFs in the 4 annuli in the V and I bands together with the best fit derived theoretical LF which sets the MF in that annulus. The errors in the observations indicated in Figures 8 and 9 are simply \sqrt{N} with N being the number of stars counted in 0.5 magnitude non-overlapping bins. The MF is characterized by its power law slope α such that $n(m) \propto m^{-\alpha}$ where n is the number of stars per unit mass and m is the mass. In general, the reduced χ^2 values for the fit between the model and the data are rather poor for most of the V LFs, and much better for those done in I . This may be a reflection of the difficulty in producing theoretical spectra of intermediate metallicity cool stars in the V -band and the greater success in the redder bands (Bedin et al. 2001, Delfosse et al. 2000). What is, however, enormously reassuring is that the power law slopes derived from the V and I data independently are in such good agreement. For the reasons stated above we adopt the I -band power law MF slopes as the value in each annulus and list these in Table 10.

To check on the effects of using different theoretical models we explored calculating the MFs using the Padova models (Girardi et al. 2000) and those of Alexander et al. (1997). These are less useful for our purposes as they are not tabulated in the HST bandpasses and the Padova models only extend down to $0.15M_{\odot}$ and not to the the hydrogen burning limit as do the other models. Since all the models were listed in Johnson V , in order to carry out the comparison we transformed $F555W$ to Johnson V (see Richer et al. 1997; Ibata et al. 1999) and compared the data with the tabulated mass – M_V relation for each of the three sets of models. We are mainly interested here in the *difference* between the derived slopes. For the outer field data (the deepest), restricting the low mass end to be $0.15M_{\odot}$ so that all 3 sets could be compared, we find that the other models produce slopes that are 0.5 (Padova) and 0.2 (Alexander) steeper than the Montalban models. If, however, we just compare the 2 sets of models that extend all the way to the hydrogen burning limit so that we can use the full range of the data, we find that the Alexander models produce a slope that has α only 0.1 larger than that of the Montalban models. We conclude from this that model choices are not a large source of systematic error in deriving the MF slopes for intermediate metallicity globular clusters. However, what is needed are a range of models from the different groups in the redder HST colors (particularly F814W) where the theory is more

successful in fitting the observations.

As can be seen in Figures 8 and 9, there is an enormous but systematic variation in the MF slopes as a function of radius. As shown here (with the $F814W$ data) and in Richer et al. (2002) with the $F606W$ images, the MF slope in the outer field is very flat with $\alpha = 0.1$. This is flatter than our result presented in Richer et al. (2002) largely because of the way the incompleteness corrections were handled. From the full matrix treatment (done here) it is clear that these corrections were somewhat over-estimated earlier. In the inner fields the slope is actually inverted taking on negative values and decreasing from -0.2 in annulus 3 through to -0.7 in the inner annulus. This is a clear signature of extensive mass segregation which we discuss in some detail in §7.

6. Towards the Hydrogen-Burning Limit in M4

We repeat here a statement made in Richer et al. (2002), namely that the least luminous MS stars observed in M4 in the outer field (where the data are deepest) are fainter than any other known subdwarf at the M4 metallicity (Leggett et al. 1998; compare LHS 1742a and LHS 377 with Figures 1 and 2 in Richer et al. 2002). We went on to conclude that a consequence of this was that there should be correspondingly faint red subdwarfs in the field waiting to be discovered. It was thus of some interest when Lépine, Rich & Shara (2003) announced the discovery of a subdwarf with properties similar to the least luminous stars found in M4.

This raises the natural question as to whether these stars are near the hydrogen-burning limit for metal-poor objects. According to the Montalbán models the lower limit for hydrogen burning at this metallicity is $0.085M_{\odot}$. The apparent $F555W$ magnitude for such a star in M4 is fainter than 35, while the apparent magnitude for stars only $0.005M_{\odot}$ more massive is fully 4.5 magnitudes brighter. This illustrates how extensively the mass-luminosity relation in the visible bands stretches out the cluster main sequence near the hydrogen-burning limit. These same models, however, suggest that deep observations in the near infra-red would be better suited than optical observations for achieving the goal of reaching the end of the main sequence. We have in hand such data from the Gemini Telescope and their reduction is currently in progress.

However, we can make some progress towards delineating the end point of hydrogen-burning in M4. For this purpose we will use the more recent deeper data taken in $F606W$ and $F814W$ from GO 8679. We note that in this data set the number of main sequence stars between our saturation limit ($F606W = 19.4$, mass $0.56M_{\odot}$) and where we start to seriously run out of stars ($F606W = 27.8$, mass $0.095M_{\odot}$) in our outer field is 520. The adopted MF slope between 0.095 and $0.56M_{\odot}$ is 0.1 and if we extend this slope to the hydrogen-burning limit at $0.085M_{\odot}$ we predict 19 stars fainter than $F606W = 27.8$. A reasonable estimate of the error in the slope is ± 0.2 given the comparison between its measured values in $F555W$ and $F814W$ from the previous section. Using this range in slope the expected numbers below $0.095M_{\odot}$ run from a low of 15 to a high of 49. We count only 6 such objects in our frames. The implication here is that if the MF continues with the same slope all the way to the bottom of the main sequence then there are at most a few tens of main sequence stars that are awaiting discovery at the faint end in this M4 field. A good test of this will be the Gemini data and whether it yields very red cluster stars not seen in the HST images.

7. Michie-King Models for M4

Our aim in constructing Michie-King models for M4 is to constrain its IMF from our data. The first task is to determine the distribution of mass within the cluster today and the second is to relate the results to plausible initial conditions. An important new constraint obtained from our work is the observed number of white dwarfs, which we have argued (Hansen et al. 2002) is a substantial fraction of the remnants formed in this cluster. A basic difficulty is that M4 has undoubtedly lost an important fraction of its initial complement

of stars through dynamical evolution and that this loss is differential: low mass stars are preferentially lost. Consequently, the interpretation of the present-day state of M4 must be guided by dynamical theory, which, as we discuss later, has only a limited capacity to address the observations of real clusters.

7.1. Comments on the Michie-King Models

Multi-mass Michie-King models (Gunn & Griffin 1979) are commonly used to convert *local* MFs determined within a field at some radial distance from the cluster center, into *global* MFs. These models, which we refer to as MMK models, are based on the assumption that each mass species can be described by a lowered Maxwell-Boltzman velocity distribution within a finite (tidal) radius. Moreover, the models are generally computed by setting the central squared velocity dispersion for each species to be inversely proportional to the species' mass. This assumption gives rise to mass segregation in the model even in the absence of strict thermal equilibrium (because the models have a finite size). The models may include velocity anisotropy but only those with an isotropic velocity distribution will be considered below.

Dynamical models usually start with an assumed homogeneous mix of stars (e.g. by setting the velocity dispersion of each species in an MMK model to a constant value) and the calculations show that well developed mass-segregation arises only very late in the evolution, generally just before core-collapse (e.g., Chernoff and Weinberg 1990). Consequently the observation of significant mass segregation, particularly a core MF that is strongly biased toward high masses, is often taken to be a sign of incipient core-collapse or perhaps a post-core-collapse state (see, e.g., Lee et al. 1991; Baumgardt and Makino 2003; hereinafter BM03). Consequently, one might be able to infer the present dynamical state of a cluster simply by comparing the degree to which the observed mass segregation is reproduced by an MMK model.

The utility of the MMK models is deceptive. Since they can involve a number of largely unconstrained parameters, they are capable, through fine tuning, of fitting almost any data set and, consequently, their predictive value is limited. In addition to the questionable assumption of imposing a thermal equilibrium condition in the standard MMK model, the applicability to real clusters is further clouded by the likely presence of unresolved binaries in the cluster core which may act as an energy source that is unaccounted for in the MMK formalism.

7.2. Constructing the Input MMK Mass Function

A basic input into the MMK models is the cluster MF which should include the observed stars, the largely unseen remnant population and any brown dwarfs.

In our MMK models, we start with a MF that is split into two power laws with slopes of α_1 for the low mass stars and α_2 for the high mass ones. The MF is assumed to match at the break point. The intent of this procedure is to mimic the shape of an IMF by converting the massive stars into remnants in a self-consistent way. In general, the break mass in this kind of formulation is a free parameter. With this construction, we obtain the following expression for the global ratio of high mass stars (N_2) to low mass stars (N_1):

$$\frac{N_2}{N_1} = \left(\frac{1 - \alpha_1}{\alpha_2 - 1} \right) \left[1 - \left(\frac{m_2}{m_3} \right)^{\alpha_2 - 1} \right] \left[1 - \left(\frac{m_1}{m_2} \right)^{1 - \alpha_1} \right]^{-1}. \quad (1)$$

In the above, m_1 , m_2 , and m_3 are the lower mass limit, the break mass, and the upper mass limit of our adopted MF. The value of N_2 is equal to the number of white dwarfs, since we assume that all stars in the upper mass range leave a remnant. Hence once we set the mass ranges, m_2/m_3 , and m_1/m_2 , in this equation,

our knowledge of α_1 and the observational constraints on the ratio of N_2/N_1 from the data permit us to find a unique solution for α_2 .

Turning first to the the low mass end, we note that there is considerable theoretical evidence that the MF at the half-mass radius is similar to the global MF (e.g., BM03), and since the half-mass radius of M4 falls very near to our outer field, we take the MF in this region to be the global MF for the main sequence stars. Hence, in accord with the results reported in §5, we adopt $\alpha_1 = 0.1$ for the present day MF over the mass range of $0.08 \leq m \leq 0.8$. the Montalban models used here place the present day turnoff mass close to $m_{to} = 0.8M_\odot$

The lower mass limit is essentially the termination mass for the hydrogen-burning main sequence and, therefore, these models do not include any brown dwarfs. If sub-stellar masses follow the observed mass function, they can have little influence on the dynamical structure and thus neglecting their existence will not affect the comparison of the model results to the observations reported here. In the absence of any clear evidence to the contrary, we prefer to set the break point in the adopted MF at the main sequence turn-off mass. We have investigated models with different break points but, as shown below, we obtain good agreement with the data for a model with the break point set at the turn-off. This is ad hoc and simply a matter of convenience. One consequence of the chosen global mass intervals, is if that $\alpha_1 + \alpha_2 = 2$, which, as we argue below, may be approximately the case in M4, then the global ratio $N_2/N_1 = 1$, implying that we might expect about half the total stellar population today to be white dwarfs.

The stars that once were above the turn-off, in the decade $0.8 \leq m \leq 8.0$, are assumed to be white dwarfs today. No neutron stars are included in the adopted cluster MF's discussed here even though M4 is known to have at least one millisecond pulsar (Lyne et al. 1988). This omission could have some effect on the very central density because the heavy neutron stars are expected, as a class, to be very centrally concentrated. The bottom heavy MFs used below would not yield very many neutron stars in the first place and many would likely recoil out of the cluster upon formation. We do not believe that the absence of neutron stars affects the modeling reported here.

In the outer field with our deepest data in *F606W* and *F814W* the number of main sequence stars (corrected for incompleteness) between masses 0.095 (*F606W* = 27.8) and $0.56M_\odot$ (*F606W* = 19.4) is 520. Extending this up to the turnoff mass at $0.8M_\odot$ with slope 0.1 as derived and down to the hydrogen-burning limit at $0.08M_\odot$ suggests a total current number of 786 (this is N_1). In our deep data in the outer field the number of white dwarfs observed to the 50% completeness limit is 290. We refer to this as N_v , rather than N_2 because these are, of course, not all the cluster white dwarfs in our field. There is certainly a population fainter than our limiting magnitude that are He white dwarfs or extremely low luminosity H-rich ones.

To account for the component of cluster white dwarfs that have not been detected, we proceed as follows. At *F606W* = 29.1 we reach the 50% completeness limit in our photometry for white dwarfs. Below this the numbers become unreliable. For a white dwarf with a typical mass ($0.6M_\odot$), the age at this luminosity is 9.5 Gyr. If we assume a cluster age of 12.1 Gyr as derived in Hansen et al. (2004), the main sequence lifetime of the progenitors of these white dwarfs was 2.6 Gyr. The mass of a star with this hydrogen-burning lifetime is $1.3M_\odot$ according to the models of Hurley et al. (2000). If we then use this mass as m_3 in equation 1 we derive from the ratio of N_v/N_1 that $\alpha_2 = 2.3$ - essentially the Salpeter slope and considerably steeper than the low mass slope in M4. Taking into account the uncertainties in the star counts, α_2 could be as low as 1.5 or as high as 2.5. In the MMK model presented below, we have used a slope of $\alpha_2 = 2.3$ applied to the entire range $0.8 - 8.0$.

The possible connection between the present-day MF and the IMF is discussed in §7.4. Here we note that the visible white dwarfs, most of which were produced in the distant past when the cluster mass was likely much higher than it is today, have a mass that is quite close to the mean mass of today's main-sequence stars. Consequently, both species will have suffered quite similar evaporative losses over the history of the cluster. In other words, we expect that the ratio of today's visible white dwarfs to today's visible main-sequence stars,

N_v/N_1 , has not changed very much and, therefore, the indicated value of α_2 is applicable to the epoch when the white dwarfs formed.

It is of interest that the derived slope is so close to the Salpeter value. Given the ubiquity of this function in Pop I environments (see, e.g., Elmegreen 2000) it perhaps is not surprising that it shows up in Pop II as well. Moreover, the flattening of the IMF at some low mass is also ubiquitous and may also be a feature of Pop II (Reid and Gizis 1999, Zoccali et al. 2000, Kroupa, 2001, Paresce and De Marchi 2000).

7.3. Constructing the Michie-King Model for M4

In an MMK model the continuous distribution of stellar masses is replaced by a series of discrete mass bins. Here, there are 12 logarithmically defined mass bins assigned to the low mass stars between 0.08 and 0.8 solar masses, and 6 to the high mass stars between 0.8 and 8.0, which include a bin between 0.8 and 1.2 to allow an easy comparison between the model and the visible white dwarfs. The stars in the high mass bins were converted to white dwarfs using Wood’s (1992) exponential initial-final mass relationship for a turn-off mass of $M_{TO} = 0.8M_{\odot}$:

$$M_{wd} = 0.510M_{\odot}e^{0.095M_{ms}}. \quad (2)$$

The mean mass of the model white dwarfs is $\langle m \rangle_{wd} = 0.56$.

Once the MF is fixed, the MMK models are a single-parameter family characterized by a normalized central potential W_0 . In addition, Each MMK model has two scale parameters that may be determined from observations of the surface brightness profile (i.e., the radial distribution of the stars): the cluster scale radius (r_s , a model parameter that approximately corresponds to the core radius, the distance where the surface density falls to about 1/2 the central value), and the projected central density. For our purposes, there is no need to independently determine that scale parameter, which would, in any case, be difficult with the data set we are using to define the cluster radial profile.

Since each mass class will have a different core radius, some care must be taken to ensure that the model mass component being fitted to the observations matches the quantity used to define the observed profile: star counts in some magnitude range or integrated light in some bandpass. Here we use surface brightness data compiled by Carlton Pryor, which includes his original counts of bright stars ($V \leq 16$) within the inner 30' of M4, supplemented by an integrated light profile from a Sky Survey photographic plate, PS-7586E, that covers the outer part of the cluster. The observed profile is that defined mainly by giants and upper main-sequence stars. In our models, we have a mass class at $0.69M_{\odot}$, which we take to represent the upper main sequence stars (including the giants), and we use the calculated radial distribution of these stars to compare with the observations.

For a given choice of r_s , we determine the best fit by spline-interpolating on the model curve at the radius of each of the observed data points and minimizing the deviation. We calculate χ^2 for the fit as the sum of $(O - C)^2/\sigma^2$, where σ is the quoted error of the data point. The star counts were fitted independently of the integrated light data at the outer radii. The difference in observational units for these two representations of the cluster profile corresponds to different density normalizations for the two data sets and, in the absence of a pre-determined connecting parameter, they must be treated separately to bring them onto our common model curve. We constructed models with W_0 between 8 and 10, and for each, varied r_c systematically to find the minimum χ^2 . The star counts were used as the determining data set; the integrated light points were used as a check. The best fit was obtained with $W_0 = 8.5$ but we note that the correlation between W_0 and r_s is such that almost indistinguishable fits could be obtained for W_0 values of 8.5 and 9.5 with slightly larger or smaller values of r_s . Our preferred fit is shown in Figure 10. The fit to the inner points (circles) has $\chi^2 = 1.28$, and the outer points (squares) have $\chi^2 = 0.92$. The scale radius for this model is $r_s = 55''$, and the *core* radius of the fitted mass-species is $r_c = 53''$, in good agreement with the Trager et al. (1993) value derived from single-mass

King models fitted to a compilation of surface-brightness data (Trager et al. 1995).

The calculated mass functions for our four annuli are plotted in Fig. 11 to show how mass segregation distorts the input global mass function in our observed fields. This plot shows the predicted number of stars per unit solar mass, per square parsec at the cluster, at the median radius of the annulus that includes each of our four fields. It is evident that if we adopt a global power law for an MMK model, then the calculated mass functions at any particular radius in the model cannot be a power law. The deviation will be particularly marked close to the cluster center, i.e., in the inner two fields, as we see plainly in Figure 11. However, we note that the model output in field 4, which is near the cluster half-mass radius, does display the global slope ($\alpha_1 = 0.1$), apart from the very highest masses. For the other fields, the power-law slopes discussed in §5 are crudely consistent with the trends observed in Fig. 11.

To connect this result back to the observed cluster luminosity functions, we proceeded as follows:

1. We used a model mass-luminosity relationship (Montalban et al. 2000) to convert the model mass to luminosity (magnitude); in other words to change the model mass function (as a function of radius) to a luminosity function (as a function of radius).
2. We spline-interpolated along the model luminosity function at each magnitude bin in the data set to get the number of stars at each luminosity.
3. We fit the model output to the observed luminosity function and compared with the data.

The result of this is shown in Figure 12 for $F555W$ and Figure 13 for $F814W$. While the χ^2 are not particularly good for $F555W$, they are acceptable for the $F814W$ luminosity functions. This demonstrates that we have achieved reasonable concordance between the presently observed M4 luminosity function and the predictions of our MMK model.

7.4. Mass Loss from M4 and Dynamical Theory: Towards the M4 IMF

The relatively shallow MF currently observed in M4 at low mass cannot be the true IMF because the cluster as a whole has suffered a substantial loss of its initial complement of stars through evaporation (e.g. Chernoff and Weinberg (1990; hereinafter CW90), (Johnstone 1993), BM03)), tidal stripping and disk-shocking (Vesperini & Heggie 1997). The mass loss due to stellar evolution is an important dynamical driver but it is the differential losses between mass species that play a critical role in the interpretation of the data. The MMK models discussed above do not include such dynamical evolution and are strictly meant to allow a comparison with the observed state of the cluster. Nevertheless, we assert that the qualitative features observed today, namely, a relatively flat MF at low masses and a remnant population that can be derived from a much steeper slope at high masses, are expected to be present in the IMF but with somewhat different quantitative values. To support our assertion, we will briefly review the present state-of-the art in the relevant aspects of the theory of cluster evolution.

The pioneering survey of the evolution of globular clusters in the Galaxy was done by CW90 using Fokker-Planck theory. Their work has been updated with an improved theoretical treatment by Takahashi and Portegies Zwart (2000 hereafter TPZ00). The basic results are mostly unchanged: clusters with top-heavy IMFs (those with most of the initial mass in rapidly evolving high-mass stars) tend to dissolve and those with bottom-heavy IMFs tend to undergo a core-collapse. The time-scales for either of these end points depends on the initial mass of the cluster, its initial central concentration, and its location in the Galaxy. The Fokker-Planck models show the expected preferential depletion of low-mass stars, which decreases the slope α of the MF at the low mass end and are the stars we observe today on the cluster lower main sequence. One important result from CW90

(their Table 6) is that changes in the MF slope are fairly small ($\Delta\alpha \simeq 0.1 - 0.3$). A second relevant point is that clusters close to core-collapse generally exhibit strong mass segregation and will exhibit a top-heavy MF in the cluster core. A third point is that clusters at their end points generally have lost between 25% and 75% of their initial mass (TPZ00). Both the CW90 and the TPZ00 models were designed to facilitate a survey of generic properties and thus do not represent any particular cluster. They assume that the IMF is a single power law between $15M_{\odot}$ and $0.4M_{\odot}$. The artificial truncation of the low-mass end of the IMF will have some quantitative effect on the evolution of bottom-heavy models but mainly it limits the comparison of these models with observational data, which now cover most of the mass decade between the turn-off at about $0.8M_{\odot}$ and the hydrogen burning limit at $0.08M_{\odot}$.

In parallel with the advances in Fokker-Planck theory, N-body studies of cluster dynamics has been greatly advanced through the development of the special purpose GRAPE machines (e.g., Makino et al. 1997). Recently, BM03 have presented the results of their extensive survey of the evolution of star clusters in the tidal field of the Galaxy. In a departure from most previous studies, they have adopted the Kroupa (2001) IMF for their work. This IMF is represented by two power laws: $\alpha_2 = 2.3$ for the high-mass end and $\alpha_1 = 1.3$ at low masses, with the break point at $0.5M_{\odot}$. These simulations included a variety of initial conditions and each model was calculated with a range of N, allowing the authors to quantify the dependence of their results on N (see Heggie 2000 and references therein for a discussion of this issue). The models were followed through core collapse to dissolution (defined as that time when 95% of the initial mass has been lost). As in the Fokker-Planck models, differential mass-loss flattens the initial MF at a slow rate until just before final disruption, a point marked by very strong mass segregation. Of particular interest is the apparent evolution of the “Kroupa kink” in the MF, which is gradually washed out and therefore, would be rather hard to detect in real data.

BM03 have applied their results to an interpretation of M4 but the theory evidently fails to reproduce the observed characteristics of M4: the observed MF is far too shallow. There are at least three plausible reasons for this failure: (1) The assumed IMF is inappropriate. Paresce and De Marchi (2000) show that a log-normal MF appears to fit most of the deep globular cluster data now available and suggest this reflects the IMF. A shallower slope ($\alpha = 0.5$) than the Kroupa value has been suggested by Reid and Gizis (1999) for the field Pop II IMF, but their value is poorly constrained. A change to a shallower slope would not likely have much affect on the BM03 results because their low-mass IMF already has the mass biased toward the high mass end. Consequently, we might expect the rate of change of the mass slope to be qualitatively similar to the published results. (2) M4 was assumed to be on a high eccentricity orbit ($\epsilon = 0.8$, Dinescu et al. 1999) moving in a logarithmic potential, appropriate to the dark matter halo only. The orbit may not be as eccentric as indicated and M4 may well be affected by tidal shocks in moving into the disk and bulge of the Galaxy. A less eccentric orbit would slow the dynamic evolution whereas tidal shocks would speed it up; the net effect is unknown. (3) The simulations did not start with a primordial binary population and any binaries that formed in the course of dynamical evolution were treated as inert. As the primordial binaries harden, they release energy that will delay the onset of core-collapse (Gao et al. 1991) and binaries that form during collapse will help power a post-core collapse expansion phase.

In light of the preceding remarks, the N-body models, like the Fokker-Planck models, are best regarded as indicative of trends. Overall, the general agreement among studies using different approaches, which, besides the above, include semi-analytical calculations (Johnstone 1993) and updated Monte-Carlo simulations (Joshi et al. 2001), is comforting. The qualitative evolution of the cluster IMF in all studies is well illustrated in Figure 7 of BM03.

The conclusions to be drawn from the observations are that M4 is in an advanced dynamical state. The evidence is the marked mass segregation and the sharply inverted mass spectrum in the central regions: it must be approaching a state of core collapse (CW90, BM03). The MMK model that describes the cluster today has 52% of the mass in the form of remnants and this high fraction is also an indication of extreme dynamical evolution (BM03). In view of the rapidity of the MF evolution toward the end of the cluster lifetime (BM03),

it is rather important to try to pin down the dynamical age. From the surveys of CW90 and TPZ03, it is likely that M4 started life in a fairly concentrated state (like the $W_0 = 7$ models in the surveys), since otherwise it would have disappeared by now given its location and orbit. Such models will typically have lost 35-70% of their initial mass (depending on the exact mass spectrum) upon entering core collapse (TPZ03). Comparing the BM03 results for their families I and II, which differ only in the adopted initial concentration ($W_0 = 5.0$ and $W_0 = 7.0$ respectively), we note that the initially more concentrated models enter core-collapse sooner and that their time to dissolution is about twice the core-collapse time. Applying this precept to M4, assuming it is about to go into core-collapse, the cluster would have a dynamical age of $T/T_{diss} \simeq 0.5$ in the notation of BM03. Removing the quasi-impulsive mass lost due to the nuclear evolution of the stars (about 30% of the initial mass for a Salpeter-like IMF), the dynamically induced mass loss is approximately linear with time. Hence this argument leads to a present day mass that is about 1/3 of its initial value. In this case the evolution of the MF slope for the present main sequence stars would still be relatively modest - typically a few tenths in the BM03 N-body models, which is similar to the predictions of the Fokker-Planck models (CW90). Hence the IMF of the low mass stars was likely quite close to being flat to begin with, say $\alpha_1 \simeq 0.4$. The location of the break mass is not discernable in our data but it is probably somewhat smaller than the turn-off mass that was adopted here. The remnant white dwarf population has a mean mass that doesn't differ too much from the mean mass of the present day main sequence stars (0.56 and $0.44M_\odot$ respectively in our MMK model) and to within a factor of order unity (CW90, Fig. 33a), both populations suffer a similar dynamically driven loss of stars. This last point alone, together with our observations, provides quite a compelling case that a steep IMF applies to the white dwarf progenitors independent of any detailed evolutionary model.

8. Summary and Discussion

The principal results from this multi-field photometric study of the main sequence of the globular cluster M4 are summarized below.

- The cluster main sequence has been traced to the limit of our data at $F555W \simeq 27.5$, $F555W - F814W \simeq 3.8$. Stars this faint are less massive than $0.1M_\odot$ according to the current generation of models.
- A simple analysis of the observed scatter about the cluster main sequence suggests a rather small overall binary fraction with weak evidence for a radially dependent binary fraction, f_b . For stars with $M_{F555W} \gtrsim 7.5$ ($M \lesssim 0.6M_\odot$), we find that $f_b \simeq 2\%$ in the cluster core but this falls to the 1% range outside. Our data thus mildly support the suggestion of (6) that M4 has a high central binary fraction which could be supplying the energy needed to prevent core-collapse in the cluster.
- The main sequence luminosity function differs significantly from field to field, and the data as a whole display a striking drop in the star counts at $F555W \simeq 24.5$.
- The local cluster mass functions determined with the Montalban et al. (2000) isochrones are quite flat in each field. The abrupt drop in the main sequence density noted above is due to the slope of the mass-luminosity relationship at low masses. The goal of reaching the end of the hydrogen-burning main sequence was not achieved here nor has it been achieved in much deeper data (Richer et al. 2002) nor in NGC 6397, the only other cluster for which such a goal is within reach (Cool et al. 1996). The existence of a minimum stellar mass is a fundamental theoretical result that can, in principle, be confirmed. Although our data appear to reach to within $\simeq 0.01M_\odot$ of the theoretical limit, the difficulty is that the mass-luminosity relationship becomes very steep as the limit is approached. The main sequence observed in the optical bands becomes very sparse and extends to extremely red colors: $(V - I) \gtrsim 5$ for the Montalban et al. (2000) models. These same calculations, however, suggest that deep observations in the near infra-red would be better suited than optical observations for achieving this goal. While there is no direct evidence that we have reached the end of the hydrogen-burning main sequence, extending the cluster mass function to this limit suggests that there are rather few cluster stars

fainter than our limiting magnitude.

- The observed variation in the cluster mass function from field to field is consistent with the segregation found in isotropic, multi-mass Michie-King models provided the present-day global mass function has a slope near the observed value of $\alpha = 0.1$. However, an accurate definition of the global cluster mass function is still not possible with the current data set. There are two reasons for this. The first has to do with the conversion of luminosity functions to mass functions through stellar models which provide the necessary mass-luminosity relationship. The models used here do not provide a reasonable fit to the extended main sequences revealed by HST observations of M4. Clearly further improvements are needed to bolster confidence in the local mass functions derived directly from the data. However, there is a suggestion that this may not be such a serious problem as the slopes derived independently from the $F555W$ and $F814W$ data are in excellent agreement. The second reason is that mass segregation occurs and, in the absence of complete radial coverage of the cluster, must be modeled to interpret the local mass functions. Multi-mass Michie-King models can be used for this purpose, as was done here. However these models have little predictive power and their applicability *as physical models* to globular clusters, particularly objects like M4, which appear to require an internal energy source to avoid core collapse, is questionable. Fortunately, the observational problem of determining the global luminosity function can be addressed simply by observing a complete radial cross-section of the cluster. HST observations are certainly needed in the core, but deep ground-based data may suffice for the halo regions. In principle, the present-day mass function can be related to the initial mass function through dynamical modeling, an ever improving art (Meylan & Heggie 1997).

An important motivation for further dynamical modeling of M4 is to provide some insight into the white dwarf remnant population now residing in the cluster. Recent steps in this direction are described in the work of Shara & Hurley (2002). As noted in Hansen et al. (2002, 2004), the cluster white dwarf luminosity function provides a new, independent age estimator. As this measurement becomes more refined, the dynamical evolution of this remnant population becomes an increasingly important issue to be understood.

A. Details of the Data Reduction

1. The data were preprocessed according to the recipe given in the ALLFRAME cookbook (Stetson 1994, Turner 1997). To summarize, vignettted regions were masked out. The images were multiplied by 4 (as this allows for short integers to be used while still sampling below the read noise) and saved as reals. They were then multiplied by an illumination map which adjusted for how each pixel was illuminated by the optics, and split into pc, wf2, wf3, wf4 fields.
2. Using a C-shell script, the ‘sky’ was measured on each image and plots made of sky-level versus sun angle (see Figure 1). This was done to investigate whether any special strategy should be employed when combining the data frames.
3. For each individual frame, we used DAOFIND with a $4\text{-}\sigma$ finding threshold to generate a star list. This list was cleaned by rejecting objects found near the edges, and the stars were photometered using PHOT and ALLSTAR. Library PSFs provided by Stetson were used.
4. During the data acquisition, the individual frames had been dithered by small pixel amounts. An initial guess was made that the frames were aligned, and this guess was refined by DAOMASTER to produce 6-term (translation and rotation) transformations between the frames (the MCH file). Note that *all* of the data, both old and new, for a given CCD was matched at the same time so that all frames were tied to the chosen reference frame.

When matching frames, the DAOMASTER program determines a magnitude offset between the frames that is later used by the MONTAGE2 program to scale frames before combining. We set this parameter

to zero. We did this as: (1) there is no variable atmospheric extinction in space; and (2) we had different filters in our matching list, which led to artificially large values of this parameter. A few images had slightly different exposure times and these were appropriately scaled.

5. The MCH file from step 4 provides geometric transformations that map the n th image in the MCH file onto the coordinate system of the first image in the MCH file (corollary: the first line in a MCH file is an identity transformation).

The MONTAGE2 program - which was designed primarily for generating finding charts from partially overlapping frames - combines the images in a MCH file by transforming and then taking a median. Instead of using MONTAGE2 to combine all of the images in our MCH file, we split our MCH file into individual lines (the n th line of the MCH file represents the geometric transformation between the n th image and the first image) and used the individual lines as input to the MONTAGE2 program. This resulted in producing (for each image in the MCH file) a new image that was on the coordinate system of the first image in the MCH file.

In summary, we transformed all the images for a given CCD to a common coordinate system, and scaled the few images which had slight differences in exposure times.

6. We combined those registered frames which had the same epoch and same filter. Four images (oldv, oldi, newv, and newi) were produced for annulus 4, whereas three images were produced (oldv, oldi, and newi) for the inner 3 annuli.

The registered frames were combined using IRAF's IMCOMBINE task to reject the brightest n pixels, and averages (not medians) were constructed of the remaining pixels. This method of combining was preferred as it provided us with higher S/N images; the noise in the average of two frames will be similar to the noise in the median of three frames (Stetson 1994). Hence, provided we reject less than 1/3 of the pixels, the noise in the high-pixel rejected averaged frame will be less than that in a median of all the data. In practice this technique allowed us to use 93% of the $F606W$ frames in the long exposures in annulus 4 and 94% of the $F814W$ images in constructing the final images. These advantages were much less spectacular for the inner annuli where the number of individual images was much less.

By rejecting high valued pixels we reject the cosmic ray events (CREs) which are present in the individual frames. The HST manual states that 20,000 pixels are affected by CREs in an 1800s exposure. This gives a CRE rate of 1.736×10^{-5} CRE pixel⁻¹ sec⁻¹. The mean number of CREs we expect in a pixel is the exposure time multiplied by 1.736×10^{-5} . As the CREs follow a Poisson distribution, the standard error of the mean is the square root of the mean. To ensure that CREs are effectively rejected, the number of pixels we reject is 5 standard deviations higher than the expected number. By visual inspection, this process was quite effective in removing cosmic ray events on our images.

7. A finding list was generated for the *combined* frames. Great care was taken in doing this by proceeding as follows:
 - (a) A 2.5 sigma find was made on the V and I frames. The resulting files were matched and stars in common to both frames were used in the initial candidate list.
 - (b) Using ALLSTAR, stars from the candidate list were subtracted from the deep V and deep I images.
 - (c) A median filter was used to smooth the unsubtracted V frame, and this median filter frame was subtracted from the V frame and the V frame without stars. These two images were displayed, stars from step 7b circled, and then the two images were blinked. With careful inspection, missed stars were added into the finding list, and spurious detections (e.g. lumps on diffraction spikes) were rejected. As a point of interest approximately 8 person-hours were expended in constructing the finding list for each chip.

- (d) the procedure in 7c was then repeated for the I frame (in order to find red objects that might have been missed on the bluer V frame), with the difference that the most recent coordinate list was used.
8. The coordinate files from step 7 were used along with Stetson’s PSFs to photometer the combined frames with the ALLSTAR program. Note that ALLSTAR has a recentering option which we enabled so as to redetermine the stellar center when performing the PSF fit.
 9. If ALLSTAR was unable to converge on the magnitude of a star, that star does not appear in the output ALLSTAR list. A consequence of this is that the ALLSTAR files from step 8 contained different subsets of the stars from the coordinate files used as finding lists. To simplify analysis, we ‘padded’ the ALLSTAR files with null data so they had a 1-to-1 correspondence with the input coordinate file (note that ALLSTAR preserves the id number used in the input coordinate file).
 10. Recall that in step 4 we matched stars on *all* frames (both new and old). As the M4 fields are dominated by cluster stars, the transformations were dominated by cluster stars (indeed, as the matching radius was decreased, the non-cluster stars were preferentially rejected). Hence, the frames were registered using primarily cluster stars. A consequence of this is that non cluster stars appear to move when frames from the two epochs are blinked. As we allowed ALLSTAR to redetermine the stellar coordinates, on a plot of $(x_{new} - x_{old})$ vs. $(y_{new} - y_{old})$ we see the cluster stars grouped around the origin, with a secondary group of non-cluster stars displaced from this.
 11. To improve the transformations between the individual frames, we generated a list of stars likely to be cluster members by isolating the clump of stars near the origin on the $(x_{new} - x_{old})$ vs. $(y_{new} - y_{old})$ diagram. A CMD of the selected stars indicated that the selection was successful. The list of candidate cluster stars is on the coordinate system of the transformed frames. We transformed this coordinate list back onto the system of each of the non-registered frames by inverting the transformation from the MCH file.
 12. Using the list of cluster stars, the individual (non-transformed) frames were reduced using the ALLSTAR program with the recenter option enabled. These ‘cluster only’ ALLSTAR files, which have only cluster candidates, were matched with DAOMASTER, using a 20 term transformation equation. By experimentation, we found that the 20 term transformation reduced systematic errors. Plots were made of dx and dy for the cluster stars, and streaming motions (indicative of a poor fit leading to large residuals) especially near the edges of the chips were seen when a 6 term transformation was used. As prescribed by Stetson, the DAOMASTER matching radius was reduced until it was similar in magnitude to the rms error in the transformation. The 20 term transformation between the frames (based on cluster stars only) was saved to a new MCH file.
 13. As in step 4, we edited the magnitude offset values in the new MCH file.
 14. As in step 5, we used the MCH file to produced transformed images. Note however that this time we used the MONTAGE2 program to expand the frames by a factor of 2 (pc CCD) or 3 (wf CCDs). The expanded, registerd images were then combined using the same procedure as described in step 6.
By expanding the frames, we found that the measured radial dispersion in the cluster proper motion was reduced from 3.9 to 2.5 mas/year. The intrinsic dispersion amongst the M4 stars is estimated to be about 0.5 mas/year, so the measured dispersion is representative of the errors associated with our technique. In effect, by expanding the frames we implemented a form of ‘drizzling’ (Fruchter & Hook 1997).
 15. A typical background value was added back to the combined frames (MONTAGE2 subtracts off the background when transforming the frames). The DAOPHOT.opt and ALLSTAR.opt files were modified to take account of the different parameters (gain, fwhm) on the expanded frame, and the master coordinate list was expanded so as to match the expanded frames.

16. Stetson’s library PSFs were not appropriate for the expanded frames, so new PSFs for these frames were built following standard techniques outlined in the DAOPHOT manual.
17. The expanded frames were photometered using ALLSTAR along with the expanded coordinate list and the PSFs built in step 16. The ALLSTAR files generated were ‘padded’ as outlined in step 9.
18. All objects in the master coordinate (.coo) list were visually classified (as to stellar or extended, isolated or possibly contaminated), and this classification was saved in the .coo file although in the final analysis no use was made of this classification.
19. As a check, a plot was made of the measured motions of the cluster stars on the sky. If the the old and new epoch are badly aligned, a ‘streaming motion’ is seen near the edges of the chips. Such a motion was noticed when a 6 term transformation was used to match the data, but this motion disappeared and the motions appeared random when the full 20 terms were used.

At this stage, the proper motion of a star (relative to the cluster) can be determined by examining its shift in x and y . Cluster stars can be isolated in the data as they will have small proper motions. An important point to note here is that in the outer annulus we were matching long exposures in $F606W$ (127.4 ksec) and $F814W$ (192.4 ksec) with much shorter exposures in $F555W$ (31.5 ksec) and $F814W$ (7.2 ksec). The question thus arises as to how we could measure positions in the earlier epoch data for the faintest stars where the s/n is obviously poor. For a star at $F606W = 29.0$ the expected s/n (from the HST ETC) in our deep $F606W$ frames is 6.7 while a star at this magnitude on the shorter exposure $F555W$ frames has s/n = 2.5. This is just about what we measured on our frames. The reason we were able to measure positions of such faint objects in the first epoch are severalfold.

First, we applied the finding list from the deep frames to the shallower frames. If the background noise in an image is Gaussian, then a 2.5σ positive deviation will occur in about 6 pixels out of every 1000. If, in a 750×750 image (neglecting the vignetted areas at the low- x and low- y sides of the WFPC2 CCDs), we were to mark all of the 2.5σ peaks as detected astronomical objects, we would expect more than 3,000 false detections. However, if we consider only the area within 0.5 pixels radius of an object confidently detected in the long second-epoch exposure, we expect a probability $\sim \pi \times 0.5^2 \times \frac{6}{1000} \approx 0.005$ of finding a positive 2.5σ deviation which is purely the result of random noise in the first-epoch image. That is to say, we expect of order 5 false cross-identifications for every 1000 correct re-detections. Even at 1.8σ , presumed re-identifications will be correct 19 times out of 20. For this reason, the knowledge that an actual astronomical object is present somewhere nearby based upon the long-exposure second-epoch images allows us to be confident that most of the claimed re-detections on the short-exposure first epoch images correspond to true re-detections. The first-epoch astrometric positions, then, while poorer than those of the second epoch, are nevertheless good enough to distinguish stars that are moving with the cluster from stars and galaxies that are not.

Secondly, the proper motions of the M4 stars are actually quite large (about 1 HST pixel with respect to an extragalactic background over the 6 year time baseline (Kalirai et al. 2003)). While the lower S/N image would not produce good enough photometry, the S/N is sufficient to give the centroid, which is crucial for astrometry. In Figure 2 we illustrated the quality of the proper motion separation between cluster and field from the long and short images in the outer field. Some of the brightest stars do not exhibit clean separation due to their near saturation. However, what is clear from this diagram is that most of the field objects can be easily eliminated down to very faint magnitudes ($F606W = 29.0$) by making the generous proper motion cut within a total value of 0.5 pixel (~ 8 mas/yr) of that of the mean cluster motion over the 6 year baseline of the observations. Since we did not push the data to its limits in this contribution, for our present purposes, we tightened this constraint to 0.3 pixels which had the effect of reducing the scatter in the resulting CMDs.

B. The Inner Halo Stars

B.1. The Inner Halo Main Sequence

The line of sight to M4 passes through the Galactic inner halo, or, perhaps more correctly, the inner Population II spheroid at a tangent radius of $R_t = R_o \sin \phi$, where $\phi = 18.3^\circ$ is the angle between the cluster line of sight and the Galactic center.

On a CMD, the stars in the inner halo will appear as a broadened sequence because they are strung out along the line of sight and may differ in age and metallicity. However, for a sufficiently steep density law, the stars will be well concentrated in a locus determined by the distance modulus of the maximum apparent stellar density. This distance, d_{max} , is slightly beyond the tangent point distance, $d(R_t) = R_o \cos \phi$, because of the increased volume sampled by the solid angle of the field of view. For the spatial density law, $\rho \sim R^{-3.5}$ (Zinn 1985), the volume correction factor is $f = d_{max}/d(R_t) = 1.061$. Therefore, the inner halo main sequence will appear below that of M4 on a CMD due to the difference in distance moduli, $\Delta\mu$, where,

$$\Delta\mu = 5 \log(f R_o \cos \phi / d_c) = 5 \log(R_o / d_c) + 0.016, \quad (\text{B1})$$

and d_c is the distance to M4.² This equation assumes that there is no additional reddening beyond M4 because the cluster is located $\simeq 500$ pc above the Galactic plane. Hence a measurement of the displacement, ΔV , between the cluster and inner halo stars on the CMD will determine the ratio R_o/d_c with an accuracy which may be much better than that attained for either R_o or d_c separately.

Inspection of the inner halo CMDs in Fig 3. (right hand panels) clearly reveals the presence of such a sequence. This inner halo main sequence is particularly well defined brighter than $V = 23$, while fainter it may be contaminated by some redder population which may be from the disk or thick disk although its kinematics are indistinguishable from that of the inner halo. The small color spread of the inner halo CMD suggests that it is meaningful to assign an average age and metallicity to this stellar population.

B.2. The M4 - Galactic Bulge Relative Distance

For a fixed age, clusters at higher metallicity will exhibit more luminous stars along the main sequence at a given color or redder stars at a given magnitude (see, e.g., the isochrones of Vandenberg & Bell 1985). An older age will go in the same direction for stars within a few magnitudes of the turnoff but this effect will be much smaller. This implies that, on the upper part of a CMD, the apparent magnitude shift between the inner halo and M4, ΔV , could differ from $\Delta\mu$, the difference in distance moduli. In general, we expect:

$$\Delta V = \Delta\mu + \alpha \Delta \log t + \beta \Delta [\text{Fe}/\text{H}], \quad (\text{B2})$$

where α and β are coefficients for positive changes in age, $\Delta \log t$, and metal abundance, $\Delta [\text{Fe}/\text{H}]$.

The magnitude of the correction terms can be obtained by appealing to isochrone calculations. For this purpose, we adopt the isochrones of Montalbán et al. (2000) which are on the HST natural system. We considered 11-15 Gyr isochrones for $[\text{Fe}/\text{H}] = -1.5, -1.3$, and -1.0 , and have simply taken averages of ratios of differences in V at fixed $V - I$ over differences in $\log t$ at a fixed $[\text{Fe}/\text{H}]$ and over differences in $[\text{Fe}/\text{H}]$ at a fixed age.

²Although a simple power law with an exponent, $n = 3.5$, characteristic of the stellar halo, may be an over-simplification of the true density distribution along the line of sight (see the discussion in Minniti 1995), the volume correction factor is quite insensitive to n : $f = 1.053$ and $f = 1.071$ for $n = 3.0$ and $n = 4.0$, respectively. This leads to less than 1% uncertainty in the distance to the stellar density maximum, a negligible amount compared to other sources of error.

The adopted values are: $\alpha \equiv dV/d\log t = 0.035$, $\beta \equiv dV/d[\text{Fe}/\text{H}] = 1.273$ so that metallicity effects will completely dominate for modest age differences. The corresponding color derivatives are $d(V-I)/d\log t = 0.007$, and, $d(V-I)/d[\text{Fe}/\text{H}] = 0.226$ so again we expect to be quite insensitive to age effects. Because of this, in what follows below, we consider only the more dominant metallicity effect. We expect that isochrones from other sources, that are constrained to provide good fits to observed globular cluster main sequences, will give similar coefficients. The results discussed below ought not to be strongly dependent on the isochrone families used in this differential way.

The main sequence associated with the inner halo was isolated by proper motion selection and contains the stars seen in the right hand panels of Figs. 3. The shifts in color and magnitude between the main sequence of the inner halo and M4 were determined as follows. Trial values of the color shift in the range $0.01 \leq \Delta(V-I) \leq 0.09$ were selected and for each value, the vertical offset was determined by an unweighted least-squares fit between the cluster and inner halo fiducials in the $(V, V-I)$ plane. The dispersion in the fit was minimized at $\Delta(V-I) = 0.05$, but values of $\Delta(V-I) = 0.04$ and 0.06 were only very slightly poorer. At $\Delta(V-I) = 0.05$, the vertical offset derived was $\Delta V = 3.5 \pm 0.07$, where the uncertainty is the formal $1-\sigma$ error in the mean value. The uncertainty in ΔV is mainly due to the difficulty in defining the inner halo fiducial, but may also reflect a slight systematic effect due to differing metallicities between the two stellar populations.

Since we are not very sensitive to age effects, we adopt $\Delta(V-I) = 0.05$ and set $\Delta\log t = 0$ as our baseline assumption. From this we obtain $\Delta[\text{Fe}/\text{H}] = 0.22$, and $\Delta\mu = 3.2 \pm 0.07$ from Eq. 2. With our preferred values for the M4 apparent distance modulus (in the $F555W$ filter) and metallicity of $\mu_c = 12.49 \pm 0.09$ and $[\text{Fe}/\text{H}]_c = -1.20$ respectively (these values are used throughout this subsection), we obtain $\mu_b = 15.69 \pm 0.11$, and $[\text{Fe}/\text{H}]_b = -0.98$ for the inner halo stars. This latter value is in quite good agreement with the results in Tiede & Terndrup (1999). A comparison between the inner halo main sequence, the M4 fiducial (which extends to high luminosity) and the isochrones (low luminosity only) interpolated to the derived metallicity and shifted to μ_b , is shown in Fig. 14. The inner halo fit and M4 fit is quite good but of course was constructed to be so. More satisfying is the agreement between the models and the inner halo which indicates that our baseline assumptions are consistent with the data. Clearly the fit degrades towards lower luminosity where it is known that the existing isochrones do not fit intermediate metallicity stellar sequences very well (Bedin et al. 2002). However, we point out that in the analysis, the models were not used in any absolute sense but only differentially to relate age and metallicity differences to variations in color and luminosity.

Fig. 14 demonstrates that we have achieved reasonable concordance of the age, metallicity and distance differences between M4 and the inner halo, through the use of the Montalban et al. (2000) isochrones. The key result from this analysis is that $\Delta\mu = 3.2 \pm 0.07$, which leads to $R_o/d_c = 4.37 \pm 0.13$. As anticipated, the formal error in this ratio is smaller than that associated with direct estimates of either R_o or d_c . The error estimate does not include any uncertainty in the observed color shift, which was fixed at $\Delta(V-I) = 0.05$ for the above estimates, nor does it include any allowance for possible age differences.

B.3. Absolute Distance Estimate to the Galactic Center

The primary motivation for the above analysis was to obtain an independent estimate of the distance to the Galactic centre from the ratio of R_o/d_c . This, of course, requires a value for d_c .

The measurement of R_o , one of the classic problems of Galactic astronomy, has been reviewed by Reid (1993). He derived a “best” value of $R_o = 8.0 \pm 0.5$ kpc from a weighted mean of the results from eight quasi-independent methods. The quoted uncertainty appears to reflect the range of values as much as the errors associated with each method. More recent discussion suggests a smaller value $R_o < 7.6$ kpc (Olling and Merrifield 2000) and the only direct measurement (Reid 1993) gives $R_o = 7.2 \pm 0.7$ kpc.

Our subdwarf based estimate of the distance to M4 is $d_c = 1.73 \pm 0.09$ kpc, which is essentially identical

to the astrometric distance ((Peterson et al. 1995)), $d_c = 1.72 \pm 0.14$ kpc. The subdwarf distance is also the same as that derived from an application of the Baade-Wesselink method to four cluster RR Lyrae stars ((Liu & Janes 1990)), $d_c = 1.73 \pm 0.005$ kpc (where the error is due only to the dispersion in absolute magnitude among the four stars used in that study).

The good agreement among the three independent estimates of the cluster distance together with the formally small errorbar associated with the subdwarf fit motivates an estimate of R_o from d_c . The result is $R_o = 7.6 \pm 0.2 \pm 0.4$ kpc, where the second, systematic error now derives from the uncertainty in our subdwarf-based estimate of d_c . With the two errors added absolutely, the relative error in this estimate of R_o is 8% and, therefore, is among the most precise of the available estimates. If the kinematic distance to M4 is used, the error, estimated in the same way, is increased to 11%, but the value of R_o (7.6 kpc) may be considered a “primary measurement” (see Reid 1993), i.e., independent of standard candles.

A basic assumption behind the above distance estimate is that the stellar density along the line of sight peaks near the tangent point, which, with $R_o = 7.5$ kpc, is $r_t = 2.4$ kpc. This distance is just inside the nominal 2.5 kpc extent of the bar detected in the infrared (Dwek et al. 1995) which is associated with the *inner* halo of the Galaxy. The bar is oriented so that the far side is projected into the same Galactic quadrant as M4. The cluster line of sight ($b = 16^\circ$) is fairly high, so the bar, as modeled by (11), falls below our tangent point and should not be a factor in this analysis. Nevertheless, poor knowledge of the spatial distribution of the stellar populations in the inner parts of the Galaxy does introduce additional systematic uncertainty in our results. An example of this may be a red population obvious in the CMD of the inner halo. This population can be seen in the right-hand panels of Fig. 3 as a redward extension of the main sequence beginning at about $V = 23$. The kinematics of this population indicates that its proper motion is consistent with that of the inner halo (i.e., distinct from that of M4) but this is not a very strong statement as the small motion of this sample with respect to an extragalactic rest frame is also similar to what one would expect from nearby disk or thick disk stars (see Kalirai et al. 2003 for further discussion).

The methodology described here is applicable to the inner halo observed behind any foreground cluster and is capable of considerable refinement with larger photometric data sets and better stellar and Galactic structure models. Given the present context, we simply note that the observed inner halo sequence is fully consistent with our adopted cluster distance and the generally accepted values for R_o .

The research of HBR is supported in part by the Natural Sciences and Engineering Research Council of Canada. HBR extends his appreciation to the Killam Foundation and the Canada Council for the award of a Canada Council Killam Fellowship. RMR and MS acknowledge support from proposal GO-8679 and BH from a Hubble Fellowship HF-01120.01 both of which were provided by NASA through a grant from the Space Telescope Science Institute which is operated by AURA under NASA contract NAS5-26555. BKG acknowledges the support of the Australian Research Council through its Large Research Grant Program A00105171.

REFERENCES

- Alcaino, G., Liller, W., & Alvarado, F. 1988, *ApJ*, 350, 569.
- Alcaino, G., Liller, W., Alvarado, F., Kravstov, V., Ipatov, A., Samus, N., & Smirnov, O. 1997, *AJ*, 114, 189.
- Alexander, D. R., Brocato, E., Cassisi, S., Castellani, V., Ciacio, F. & Degl’Innocenti, S., 1997, *A&A*, 317, 90
- Baumgardt, H., Makino, J. 2003, *MNRAS*, 340, 227.
- Bedin, L.R., Anderson, J., King, I.R., & Piotto, G. 2001, *ApJ*, 560, L75.
- Bedin, L.R., G., King, I.R., & Anderson, J. 2003, *AJ*, 126, 247.
- Bessell, M.S. 1996, *PASP*, 107, 672.
- Burrows, A., Hubbard, W.B., Saumon, D., & Lunine, J.I. 1993, *ApJ*, 406, 158.
- Cardelli, J.A., Clayton, G.C., & Mathis, J.S. 1989, *ApJ*, 345, 245.
- Carney, B.W. 1996, *PASP*, 108, 900.
- Carretta, E. & Gratton, R.G. 1997, *A&A Suppl*, 121, 95.
- Chernoff, D.F., & Weinberg, M.D. 1990, *ApJ*, 351, 121.
- Cohn, H. 1980, *ApJ*, 242, 765.
- Cool, A.M., Piotto, G., & King, I.R. 1996, *ApJ*, 468, 655.
- Côté, P., & Fischer, P. 1996, *AJ*, 112, 165.
- Cudworth, K.M. & Rees, R. 1990, *AJ*, 99, 1491,
- Dauphole, B., Geffert, M., Colin, J., DuCourant, C., Odenkirchen, M., & Tucholke, H-J. 1996, *A&A*, 313, 119.
- Delfosse, X., Forveille, T., Ségranson, D., Beuzit, J.-L., Udry, S., Perrier, C., & Mayor, M. 2000, *A&A*, 364, 217.
- Dixon, R.I., & Longmore., A. 1993, *MNRAS*, 265, 395.
- Djorgovski, S.G. 1993, in “ Structure and Dynamics of Globular Clusters”, ASP Conference Series, Vol. 50, eds. S.G. Djorgovski & G. Meylan, (San Francisco:ASP), p. 373.
- Drake, J.J., Smith, V.V., & Suntzeff, N.B. 1994, *ApJ*, 430, 610.
- Drukier, G.A., Fahlman, G.G., & Richer, H.B. 1992, *ApJ*, 386, 106.
- Dwek, E., Arendt, R.G., Hauser, M.G., Kelsall, T., Lisse, C.M., Moseley, S.H., Silverberg, R.F., Sodroski, T.J., & Weiland, J.L. 1995, *ApJ*, 445, 716.
- Elmegreen, B.G. 2000, *ApJ*, 539, 342.
- Fahlman, G.G., Richer, H.B., & Nemeč, J. 1991, *ApJ*, 380, 124.
- Fahlman, G.G., Richer, H.B., Ibata, R.I., Ivanans N.C., Mandushev, G., Hesser, J.E., Stetson, P.B. Wood, M.A., Pryor, C., Harris, W.E., Bond, H.E., Bolte, M.B., & Bell, R.A. 1996a, in “Dynamical Evolution of Star Clusters – Confrontation of Theory and Observations”, IAU Symp. 174, eds J. Makino & P. Hut (Dordrecht:Reidel), p. 39.

- Fahlman, G.G., Mandushev, G.G., Richer, H.B., Thompson, I.B., & Sivaramakrishnan, A. 1996b, *ApJ*, 459, L65.
- Ferdman, R.D., Brewer, J., Fahlman, G.G., Gibson, B.K., Hansen, B.M.S., Huber, M.E., Ibata, R.I., Kalirai, J.S., Matthews, J.M., Rich, R.M., Richer, H.B., Rowe, J.F., Shara, M.M., & Stetson, P.B. 2003, *astro-ph/0304470*.
- Frogel, J.A., Persson, S.E., & Cohen, J.G. 1981, *ApJ*, 246, 842.
- Fruchter, A., & Hook, R.N. 1997, *SPIE* 3164, 120.
- Girardi, L., Bressan, A., Bertelli, G., & Chiosi, C. 2000 *A&AS*, 141, 371
- Gizis, J.E. & Reid, I.N. 1999, *AJ*, 117, 508.
- Goa, B., Goodman, J., Cohn, H., & Murphy, B. 1991, *ApJ*, 370, 567.
- Gunn, J. & Griffin, R.F. 1979, *AJ*, 84, 752.
- Hansen, B.M.S., Brewer, J., Fahlman, G.G., Gibson, B.K., Ibata, R., Limongi, M., Rich, R.M., Richer, H.B., Shara, M.M., & Stetson, P.B. 2002, *ApJ*, 574, L155.
- Hansen, B.M.S., Richer, H.B., Fahlman, G.G., Stetson, P.B., Brewer, J., Currie, T., Gibson, B.K., Ibata, Rich, R.M. & Shara, M. 2004, *ApJ*, submitted.
- Heggie, D.C. 2000, presented at the International Conference of the Astronomische Gesellschaft at Heidelberg, March 20-24, 2000, talk #02.
- Holtzman, J.A., Burrows, C.J., Hester, J., Traiger, J.T., Watson, A.M., & Worthey, G. 1995, *PASP*, 107, 1065.
- Ibata, R.I., Richer, H.B., Fahlman, G.G., Bolte, M., Bond, H.E., Hesser, J.E., Pryor, C., & Stetson, P.B. 1999, *ApJS*, 120, 265. (Paper II)
- Johnstone, D. 1993, *AJ*, 105, 155.
- Joshi, K.J., Nave, C.P. & Rasio, Frederic A. 2001, *ApJ*, 550, 691.
- Hurley, J.R., Pols, O.R. & Tout, C.A. 2000, *MNRAS* 315, 543.
- Kalirai, J.S., Richer, H.B., Hansen, B.M., Stetson, P.B., Shara, M.M., Saviane, I., Rich, R.M., Limongi, M., Ibata, R., Gibson, B.K., Fahlman, G.G., & Brewer, J. 2003, *astro-ph/0306241*.
- Kanatis, I.N., Griffiths, W.K., Dickens, R.J., & Penny, A.J. 1995, *MNRAS*, 272, 265.
- Kroupa, P. 2001, *MNRAS*, 322, 231.
- Leggett, S.K. Allard, F., & Hauschildt, P.H. 1998, *ApJ*, 509, 836.
- Lépine, S., Rich, R.M., & Shara, M. 2003, *ApJ*, 591, L49.
- Liu, T. & Janes, K.A. 1990, *ApJ*, 360, 561.
- Lyne, A.G., Biggs, J.D., Brinklow, A., McKenna, J., & Ashworth, M. 1988, *Nature*, 332, 45.
- Lyons, M.A., Bates, B., Kemp, S.N., & Davies, R.D. 1995, *MNRAS*, 277, 113.
- Mandushev, G.I., Fahlman, G.G., Richer, H.B., & Thompson, I.B. 1996, *AJ*, 112, 1536.

- Meylan, G. & Heggie, D.C. 1997, *A&ARev.*, 8, 1.
- Montalban, J., D’Antona, F., & Mazzitelli, I. 2000, *A&A*, 360, 935.
- Murphy, B.W. & Cohn, H. 1988, *MNRAS*, 232, 835.
- Olling, R.P., & Merrifield, M.R. 2000, *MNRAS*, 311, 361.
- Paresce, F. & De Marchi, G. 2001, *ApJ*, 534, 870.
- Perryman, M.A.C., Lindegren, L., Kovalevsky, J., Hog, E., Bastian, U., Bernacca, P.L., Creze, M., Donati, F., Grenon, M., Grewing, M., Van Leeuwen, F., Van Der Marel, H., Mignard, F., Murray, C.A., Le Poole, R.S., Schruver, H., Turon, C., Arenou, F., Froeschle, M., & Petersen, C.S. 1997, *A&A*, 323, L49.
- Peterson, R.C., Rees, R.F., & Cudworth, K.M. 1995, *ApJ*, 443, 124.
- Piotto, G., Cool, A.M., & King, I.R. 1997, *AJ*, 113, 1345.
- Piotto, G., & Zoccali, M. 1999, *A&A*, 345, 485.
- Pryor, C., Fletcher, J.M., Hesser, J.E., McClure, R.D., Stetson, P.B., Richer, H.B., Fahlman, G.G., Ibata, R.A., Ivanans, N.C., Mandushev, G.M., Bell, R.A., Bolte, M., Bond, H.E., Harris, W.E., VandenBerg, D.A., & Wood, M.A. 1996, in “Dynamical Evolution of Star Clusters – Confrontation of Theory and Observations”, *IAU Symp.* 174, eds J. Makino & P. Hut (Dordrecht:Reidel), p. 39.
- Pryor, C., & Meylan, G. 1993, in “Structure and Dynamics of Globular Clusters”, Proceedings of a Workshop held in Berkeley, California, July 15-17, 1992, to Honor the 65th Birthday of Ivan King. Editors, S.G. Djorgovski and G. Meylan; Publisher, Astronomical Society of the Pacific, Vol. 50, San Francisco, California, p. 357.
- Pulone, L., de Marchi, C., & Paresce, F. 1999, *A&A*, 342, 440.
- Reid, M.J. 1993, *ARA&A*, 31, 345.
- Richer, H.B. & Fahlman, G.G. 1984, *ApJ*, 277, 227.
- Richer, H.B. & Fahlman, G.G. 1989, *ApJ*, 339, 178.
- Richer, H.B., Fahlman, G.G., Ibata, R.A., Stetson, P.B., Bell, R.A., Bolte, M., Bond, H.E., Harris, W.E., Hesser, J.E., Mandushev, G., Pryor, C., & VandenBerg, D.A. 1995, *ApJ*, 451, L17.
- Richer, H.B., Fahlman, G.G., Ibata, R.A., Ivanans, N.C., Mandushev, G.M., Hesser, J.E., Stetson, P.B., VandenBerg, D.A., Pryor, C., Harris, W.E., Bond, H.E., Bolte, M., & Bell, R.A. 1996a, in “The Origins, Evolutions and Destinies of Binary Stars in Clusters”, eds E.F. Milone, & J-C Mermillod, *ASP Conference Series*, Vol. 90, p. 65.
- Richer, H.B., Harris, W.E., Fahlman, G.G., Bell, R.A., Bond, H.E., Hesser, J.E., Holland, S., Pryor, C., Stetson, P.B., VandenBerg, D.A., & van den Berg, S. 1996b, *ApJ*, 463, 602.
- Richer, H.B., Fahlman, G.G., Ibata, R.A., Pryor, C., Bell, R.A., Bolte, M., Bond, H.E., Harris, W.E., Hesser, J.E., Holland, S., Ivanans, N.C., Stetson, P.B., & Wood, M. 1997, *ApJ*, 484, 741, 1997.
- Richer, H.B., Brewer, J., Fahlman, G.G., Gibson, B.K., Hansen, B.M.S., Ibata, R., Kalirai, J.S., Limongi, M., Rich, R.M., Richer, H.B., Saviane, I., Shara, M.M., & Stetson, P.B. 2002, *ApJ*, 574, L151.
- Rutledge, G.A., Hesser, J.E., & Stetson, P.B. 1997, *PASP*, 109, 907.

- Shara, M.M. & Hurley, J.R. 2002, *ApJ*, 571, 830.
- Stetson, P.B. 1994, *PASP*, 99, 613.
- Takahashi, K. & Portegies Zwart, S.F. 2000, *ApJ*, 535, 759.
- Tiede, G.P., & Terndrup, D.M. 1999, *AJ*, 188, 895.
- Trager, S.C., Djorgovski, S., & King, I.R. 1993, in “Structure and Dynamics of Globular Clusters”, *ASP Conference Series*, Vol. 50, eds. S.G. Djorgovski & G. Meylan, (San Francisco:ASP), p. 347.
- Trager, S.C., King, I.R., & Djorgovski, S. 1995, *AJ*, 109, 218.
- Turner, A., 1997, *Cooking with ALLSTAR*.
- VandenBerg, D.A. & Bell, R.A. 1985, *ApJS*, 58, 561.
- Vesperini, E. & Heggie, D.C. 1997, *MNRAS*, 289, 898.
- Vrba, F.J., Coyne, G.V., & Tapia, S. 1993, *AJ*, 105, 1010.
- Wood, M.A. 1992, *ApJ*, 386, 539.
- Zinn, R. 1985, *ApJ*, 293, 424.
- Zoccali, M., Cassisi, S., Frogel, J.A., Gould, A., Ortolani, S., Renzini, A., Rich, R.M. & Stephens, A.W. 2000, *ApJ*, 530, 418.

Fig. 1.— The variation in the sky background as a function of time (Mean Julian Days) or angle between the Sun and M4 on the long exposure frames in the outer annulus in both $F606W$ and $F555W$. The decrease is due to the lowering of the zodiacal light background as the Sun-M4 angle increased. The few jumps in the brightness levels are due to observations taken close to the bright limb of the Earth.

Fig. 2.— Total proper motion difference between M4 and background/foreground objects as a function of magnitude for the outer field data. In this diagram the motion is zero-pointed on M4 and the displacement is given in HST pixels over the 6 year baseline of the observations. In order to separate the cluster from the field all objects possessing motion within 0.5 pixel of that of M4 were assumed to be cluster members. Because we do not resolve the M4 internal motion, it is clear from the diagram that our uncertainties in the measured proper motions do not exceed 2 mas/yr down to $F606W = 27.5$ and at $F606W = 29.5$ they are smaller than 7 mas/yr.

Fig. 3.— All stars within the 4 annuli selected by proper motion are plotted in the sequence $a - d$ with a being the inner annulus. The upper section of each plot is the proper motion selection with the units being relative motion in HST pixels ($0.1''$) over the 6 year time baseline. The densest and most concentrated clump consists of the M4 stars and their CMD is illustrated in the left hand panels. The right hand sequence is largely due to stars in the inner halo of the Galaxy. The cluster main sequence is the reddest of the sequences observed in these plots, the cluster white dwarfs are the bluest sequence.

Fig. 4.— The magnitude of the average photometric errors in the inner annuli (1-3) in both I and V from artificial star tests are plotted as a function of stellar magnitude.

Fig. 5.— CMDs in the 4 annuli with the cluster main sequence fiducial shifted brighter by 0.75 mags in order to indicate the location of an equal-mass binary sequence. Saturation is important for $F555W < 20$ particularly in the outer field. It appears from this diagram that the equal mass cluster binary frequency is very low.

Fig. 6.— A simulation of the binary frequency in our fields. The stars were drawn at random from mass functions with the indicated slopes and assigned errors as in Fig. 4. Figures 5 and 6 collectively suggest a modest main sequence binary frequency in our M4 fields.

Fig. 7.— Histograms of the deviation of M4 stars (in magnitudes) from the main-sequence fiducial. Small excesses are clearly seen towards negative residuals at about 0.75 magnitudes in the inner 2 annuli suggesting a photometric main sequence binary frequency of a few percent.

Fig. 8.— Observed cluster luminosity functions (points with error bars) in V compared with the theoretical function derived from the best fitting mass function. The mass function slopes ($\alpha_{Salpeter} = +2.3$) and χ^2 fit between theory and observed function are indicated.

Fig. 9.— As in Fig. 8 except that the functions are developed from the I magnitudes and are independent of those in V . The agreement in mass function slopes between the two bandpasses in the same annuli is remarkably good.

Fig. 10.— The M4 surface brightness profile defined by counts of stars with $V < 16$ (symbols with error bars) is compared to the profile of a corresponding mass-class from the MMK model adopted here. The best fit occurs for a scale radius, $r_s = 55''$.

Fig. 11.— The mass functions predicted by the MMK model in our 4 annuli are shown. The mass function in annulus 4 (A4) reproduces the input global mass function, except for the very highest masses, which were not observed here and are predicted to be somewhat segregated toward the cluster center. The calculated mass functions in the inner annuli are not power laws but, nevertheless, are crudely consistent with the power law slopes derived in §5 of the text. A comparison of the model predictions to the observed luminosity functions is

provided in Fig. 12.

Fig. 12.— Model luminosity functions in V in the 4 annuli compared to the data (points with error bars). This diagram indicates that we have achieved reasonable agreement between the M4 luminosity functions and those expected in equilibrium MMK models.

Fig. 13.— As in Fig. 12 except that the luminosity functions here are derived from the I -band data.

Fig. 14.— Left hand panel: The M4 CMD in the inner 3 annuli. Right hand panel: The CMD of non-cluster stars (largely inner halo) in the direction of M4 from the 3 inner annuli. This inner halo main sequence is compared to the M4 fiducial (the fiducial has been extended to brighter magnitudes using ground-based data) and the isochrones (bluest at low luminosity) interpolated to the derived metallicity and both shifted to a distance modulus of 3.2 magnitudes larger than that of the cluster.

Table 1. M4 Physical Parameters

Parameter	Value	Comment	Reference
distance (kpc)	1.73 ± 0.09	Subdwarf fit	1
	1.72 ± 0.14	Astrometric	2
	1.72 ± 0.01	Baade-Wesselink	3
true distance modulus	11.18	as above	1,2,3
E(V-I)	0.51 ± 0.02	Subdwarf fit (Johnson Colors)	1
R_V	3.8	Observed extinction (Johnson Colors)	2,3,4,5
A_V	1.33	Model extinction curves (Johnson Colors)	6
A_{F555W}	1.31	Model extinction curves	6
A_{F814W}	0.82	Model extinction curves	6
[Fe/H]	-1.20 ± 0.15	Spectroscopy	7
core radius (r_c)	53''	King model	8,11
concentration (c)	1.74	King model	10
half light radius (l_{rh})	269''	King model	8
half mass radius (m_{rh})	367''	King model	11
integrated luminosity (\mathcal{L}_V)	$6.25 \times 10^4 L_\odot$	photometry	9,11
central Mass/Light (\mathcal{M}/\mathcal{L}) ₀	1.64	King model	11
global Mass/Light (\mathcal{M}/\mathcal{L})	1.00	King Model	10, 11
relaxation time (t_{rh})	2.18×10^8 yr.	Spitzer formula	9,11
central relax. time (t_{rc})	1.80×10^7 yr.	Spitzer formula	9,11

References. — (1) Richer *et al.* 1997 (Paper I); (2) Peterson *et al.* 1995; (3) Liu & Janes 1990; (4) Dixon & Longmore 1993; (5) Vrba *et al.* 1993; (6) Cardelli *et al.* 1989; (7) Drake *et al.* 1994; (8) Trager *et al.* 1993; (9) Djorkovski 1993; (10) Pryor & Meylan 1993; (11) this paper.

Table 2. Field Geometry

Annulus	inner r_c	outer r_c	median '	area \square'
1	0	1.5	0.938	1.75
2	1.5	2.5	1.625	2.87
3	2.5	4.0	2.522	2.73
4	4.0	...	5.028	4.98

Table 3. Exposure Record

Field(r_c)	Date	Program ID	Filter	Exposure	Number of frames	Comments
1	1995	5461	F336W	1300	1	
1	1995	5461	F336W	1500	7	
1	1995	5461	F555W	1000	15	
1	1995	5461	F814W	600	1	first epoch for pm
1	1995	5461	F814W	700	7	first epoch for pm
1	2000	8153	F814W	700	8	second epoch for pm
2	1995	5461	F336W	1300	1	
2	1995	5461	F336W	1500	7	
2	1995	5461	F555W	1000	15	
2	1995	5461	F814W	600	1	first epoch for pm
2	1995	5461	F814W	700	7	first epoch for pm
2	2000	8153	F814W	700	8	second epoch for pm
6	1995	5461	F555W	2100	15	first epoch for pm
6	1995	5461	F814W	800	9	first epoch for pm
6	2001	8679	F606W	1300	98	second epoch for pm
6	2001	8679	F814W	1300	148	second epoch for pm

Table 4. Annulus 1: Photometry and Astrometry^a

RA	DEC	F555W	F814W	$\mu_{\alpha\cos(\delta)}$	μ_{δ}
245.8968	-26.5372	19.712	18.236	-13.740	-19.528
245.8971	-26.5371	19.615	18.139	-14.558	-20.437
245.8977	-26.5388	23.041	20.449	-12.390	-18.678
245.8978	-26.5365	21.049	19.136	-12.431	-17.723
245.8978	-26.5386	22.851	20.470	-14.528	-20.200

^aThis is just the first 5 entries in this table which can be retrieved in full from the Astronomical Journal Archives.

Table 5. Annulus 2: Photometry and Astrometry^a

RA	DEC	F555W	F814W	$\mu_{\alpha}\cos(\delta)$	μ_{δ}
245.9035	-26.5467	21.001	19.157	-11.547	-17.889
245.9036	-26.5457	23.862	21.316	-14.084	-18.983
245.9041	-26.5464	20.320	18.630	-11.496	-19.782
245.9042	-26.5465	23.886	22.975	-11.920	-19.095
245.9050	-26.5456	20.600	18.817	-11.154	-19.344

^aThis is just the first 5 entries in this table which can be retrieved in full from the Astronomical Journal Archives.

Table 6. Annulus 3: Photometry and Astrometry^a

RA	DEC	F555W	F814W	$\mu_{\alpha\cos(\delta)}$	μ_{δ}
245.9183	-26.4944	24.773	22.198	-12.803	-17.138
245.9184	-26.4946	23.042	20.727	-13.528	-16.526
245.9194	-26.4951	20.653	18.888	-13.127	-17.936
245.9196	-26.4956	22.404	20.254	-11.859	-16.632
245.9200	-26.4943	27.027	25.723	-13.396	-17.554

^aThis is just the first 5 entries in this table which can be retrieved in full from the Astronomical Journal Archives.

Table 7. Annulus 4: Photometry and Astrometry^a

RA	DEC	F555W	F814W	$\mu_{\alpha\cos(\delta)}$	μ_{δ}
245.9678	-26.5533	22.027	20.140	-11.631	-19.955
245.9680	-26.5538	22.111	20.044	-11.374	-19.479
245.9695	-26.5511	25.209	24.284	-13.151	-16.950
245.9695	-26.5516	28.134	26.669	-8.621	-14.968
245.9701	-26.5515	22.273	20.152	-13.651	-19.347

^aThis is just the first 5 entries in this table which can be retrieved in full from the Astronomical Journal Archives.

Table 8. Main Sequence Fiducial

$F555W - F814W$	$F555W$
1.384	19.368
1.455	19.650
1.525	19.888
1.596	20.102
1.667	20.312
1.737	20.525
1.808	20.749
1.878	20.992
1.949	21.264
2.020	21.563
2.090	21.885
2.161	22.224
2.232	22.567
2.302	22.901
2.373	23.228
2.444	23.542
2.514	23.831
2.585	24.086
2.655	24.320
2.726	24.550
2.797	24.783
2.867	25.020
2.938	25.268
3.009	25.532
3.079	25.806
3.150	26.048
3.221	26.238
3.291	26.394
3.362	26.538
3.432	26.687
3.503	26.843

Table 9. Upper Limits on M4 Binary Fractions

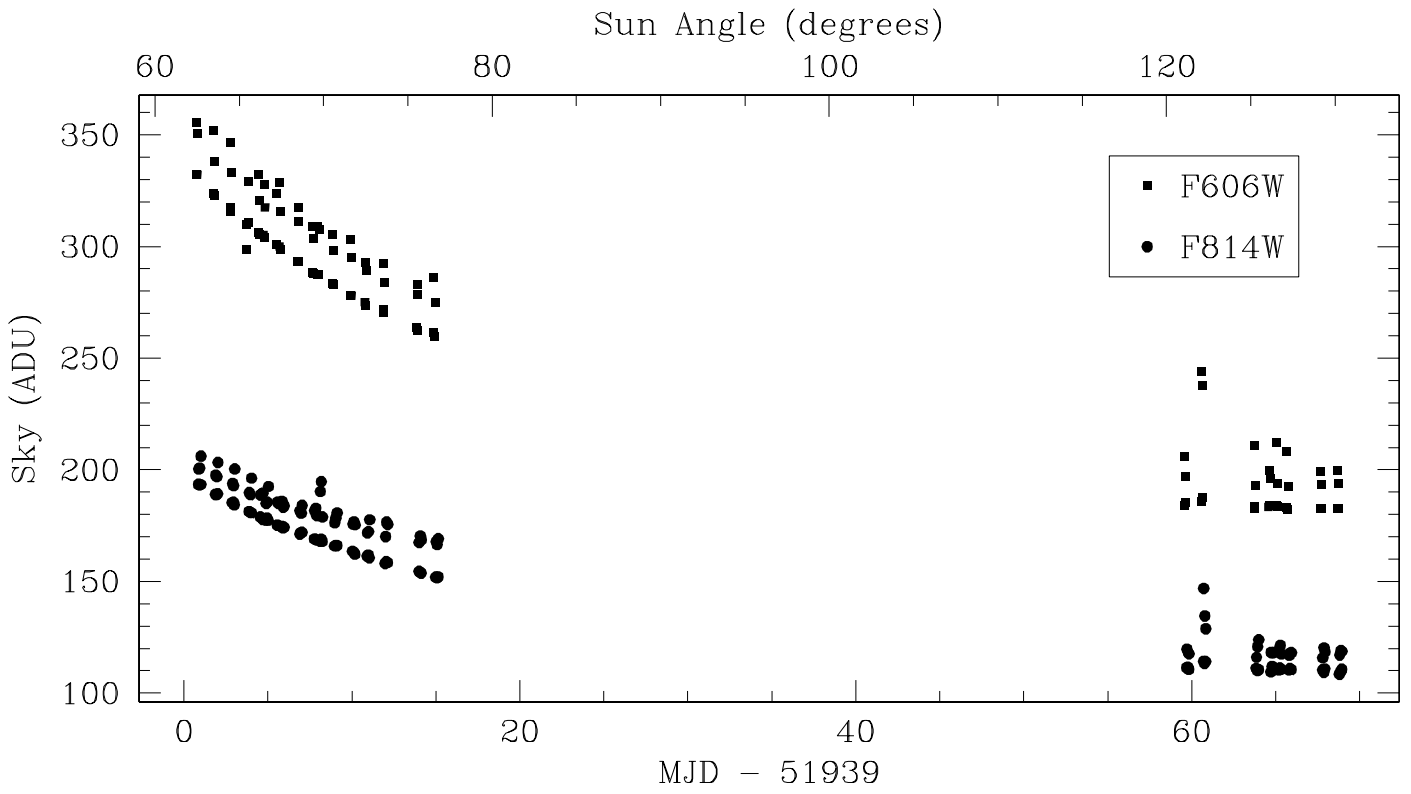
Annulus	f_b (%)	$\pm\sigma$	Number ^a
1	2.2	0.8	403
2	1.1	0.4	805
3	1.1	0.3	759
4	1.8	0.5	514

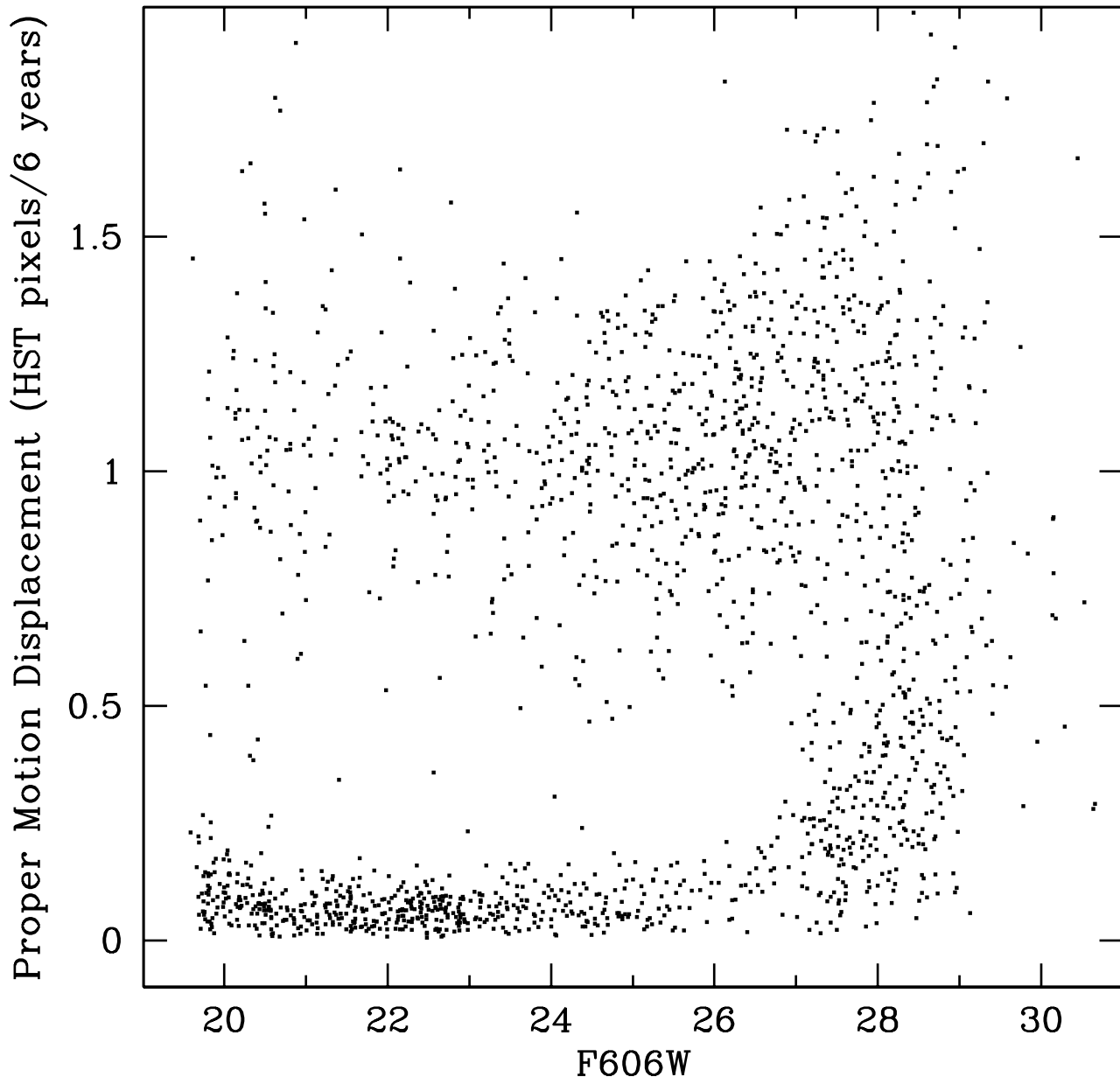
^aThe total number of main sequence stars used.

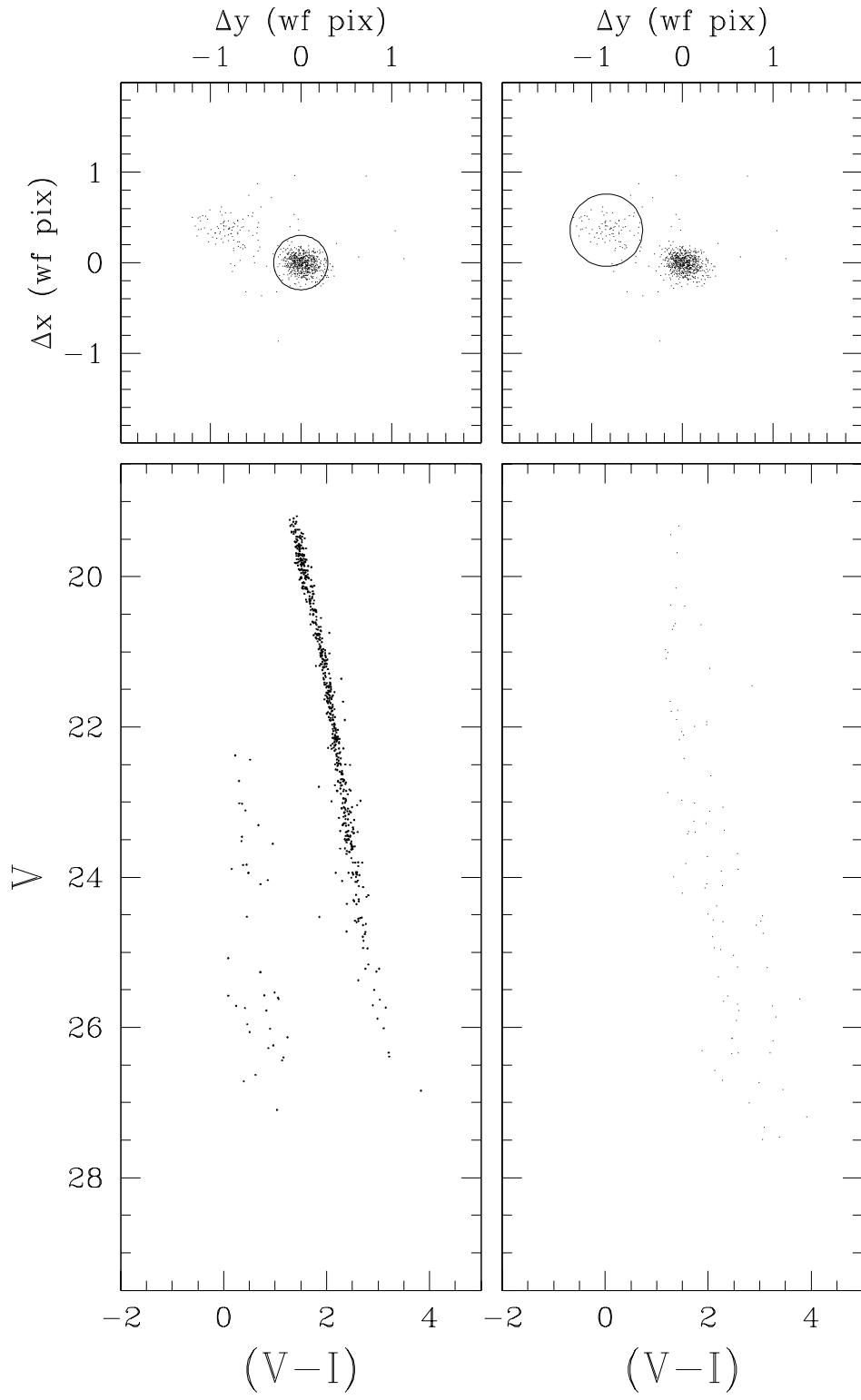
Table 10. Mass Function Slopes at Different Radii

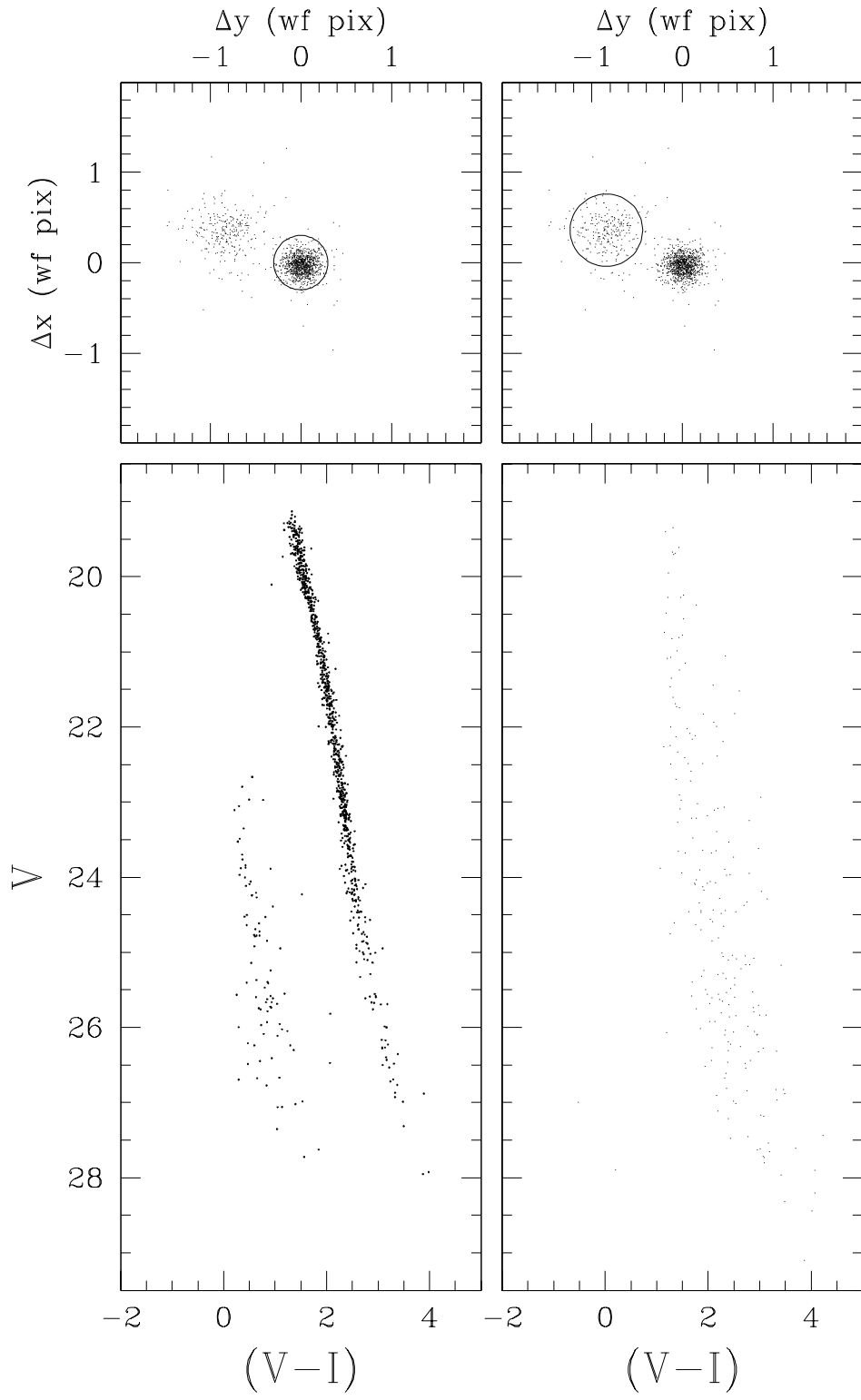
Annulus	r/r_h^a	$\alpha_{observed}$
1	0.17 ± 0.09	-0.7
2	0.30 ± 0.09	-0.4
3	0.47 ± 0.14	-0.2
4	0.94 ± 0.19	0.1

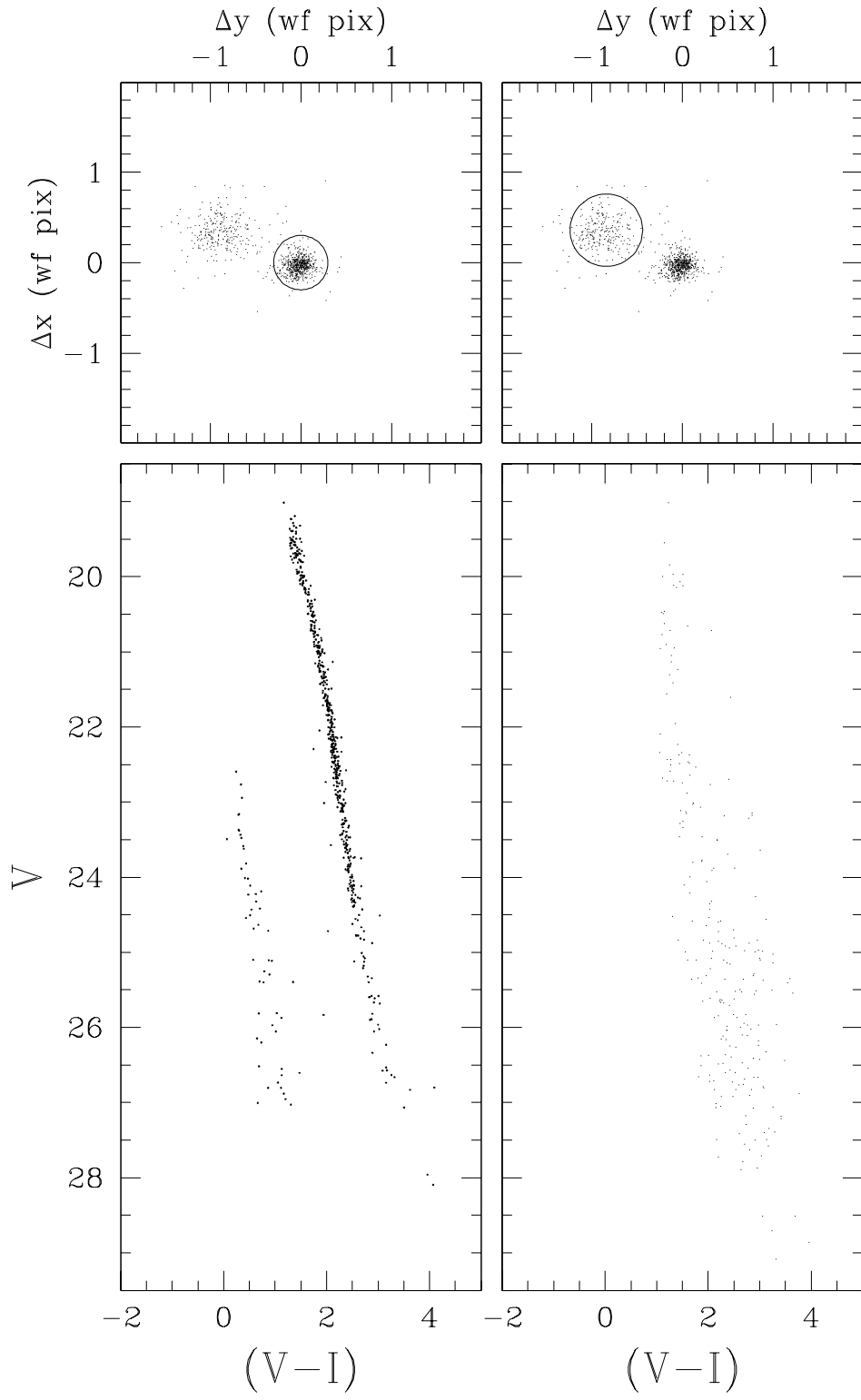
^a $r_h = 269''.2$ from Trager et al. (1993)

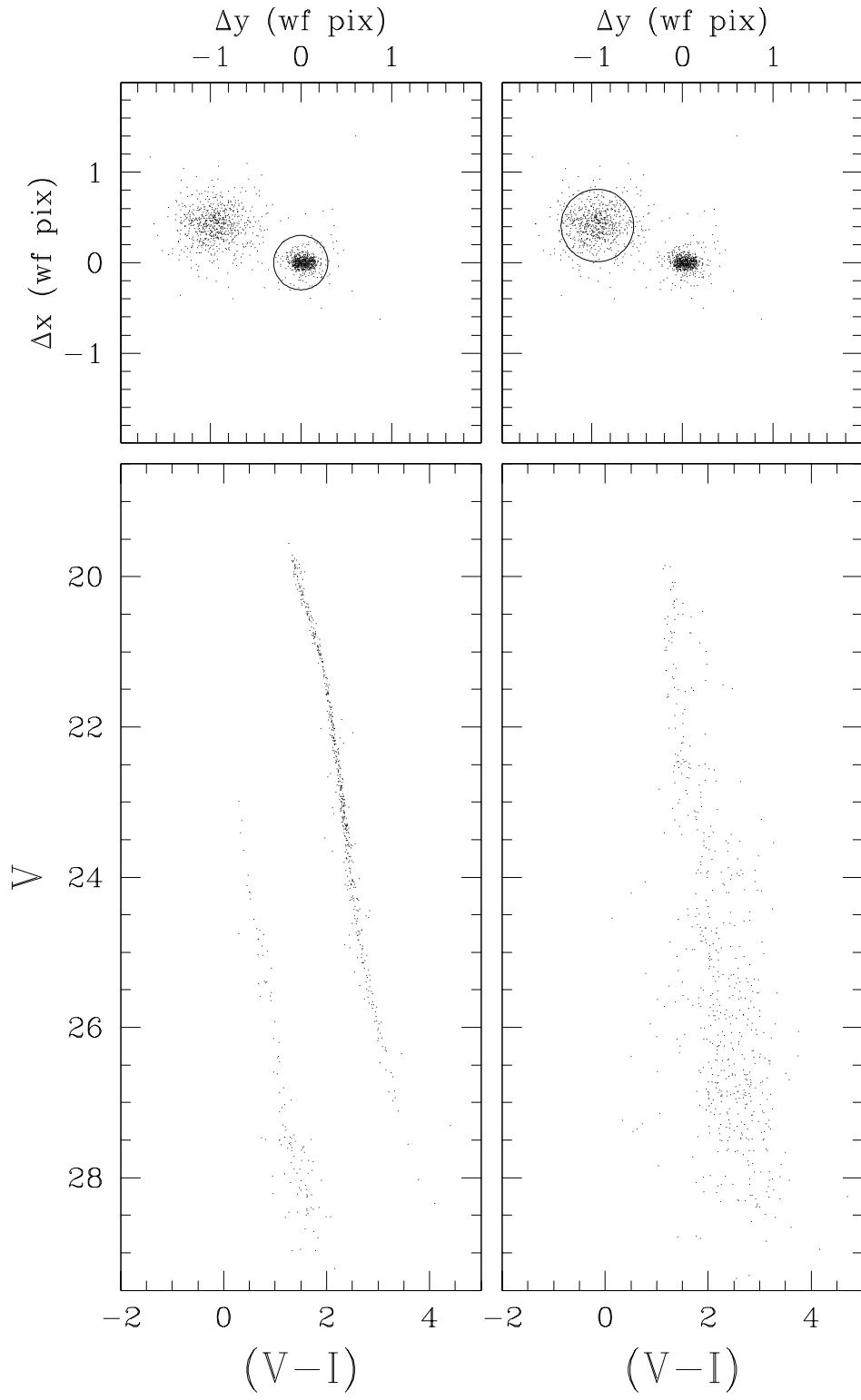


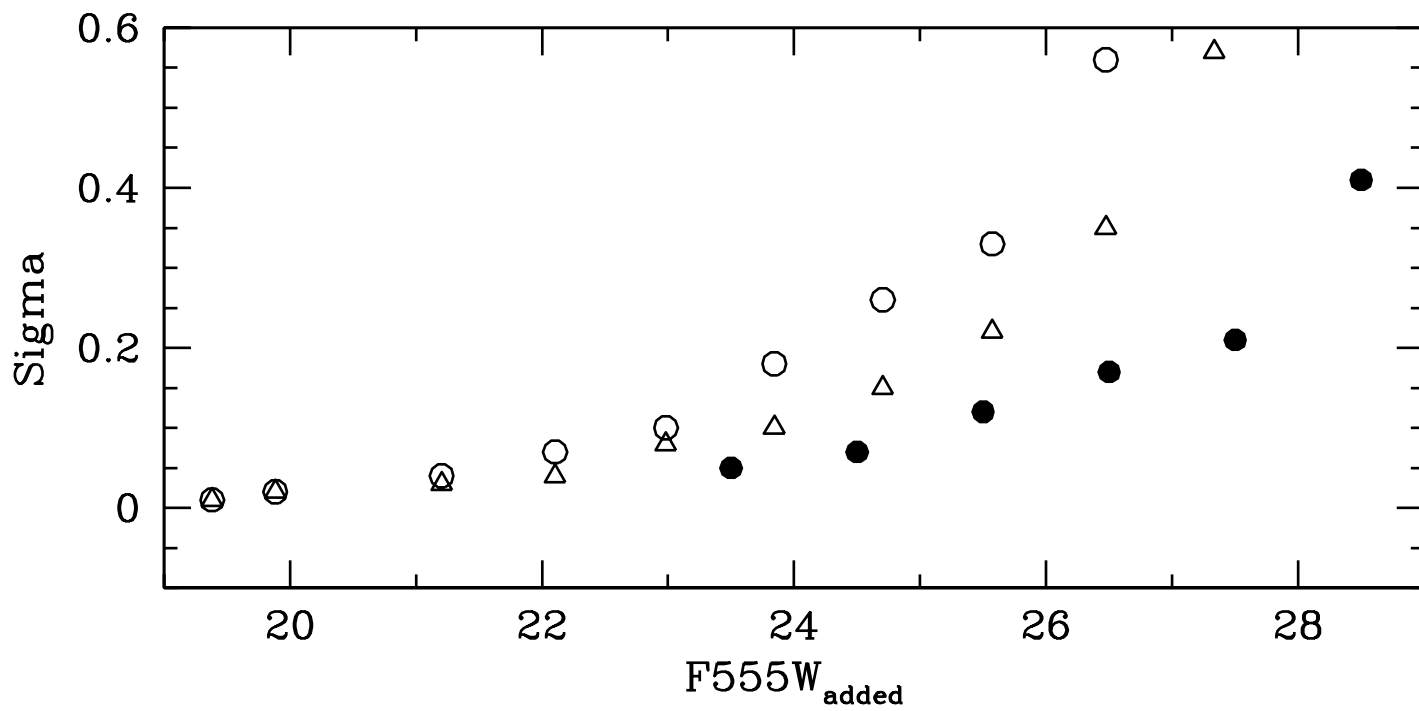
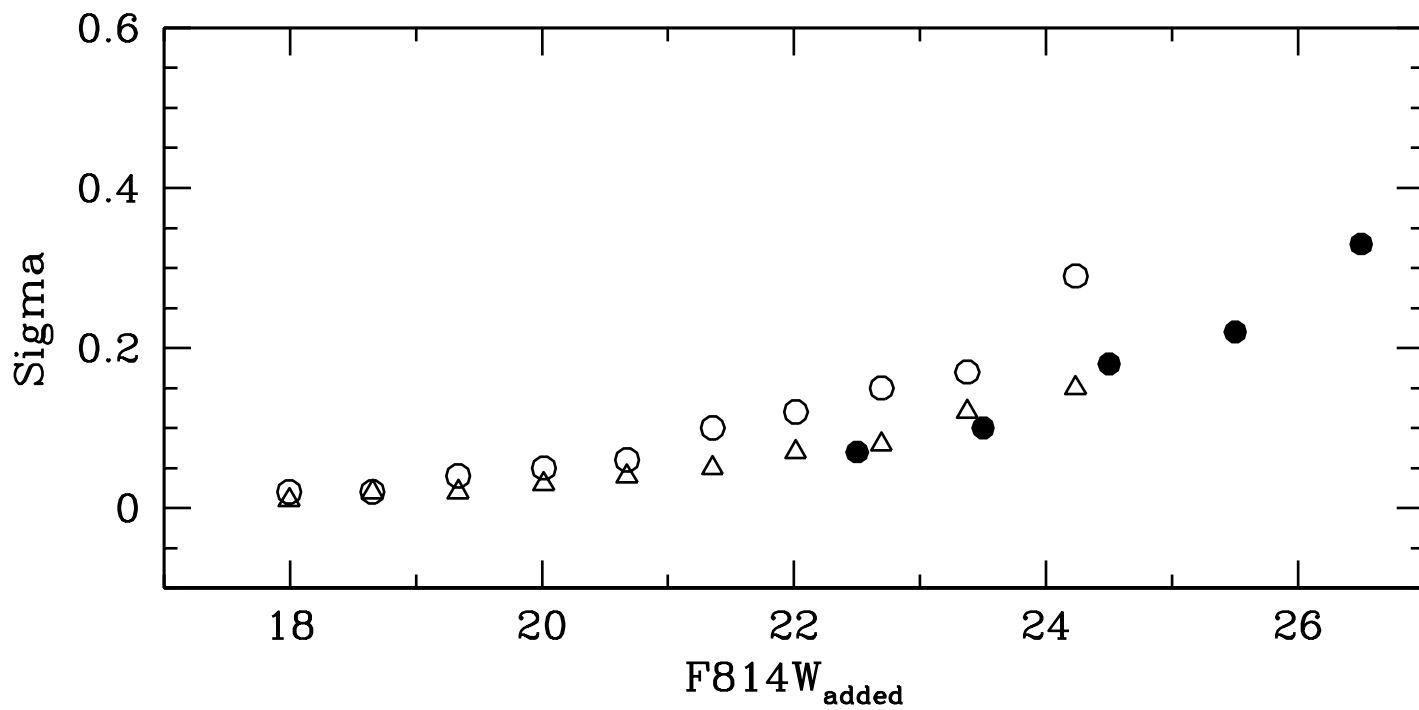


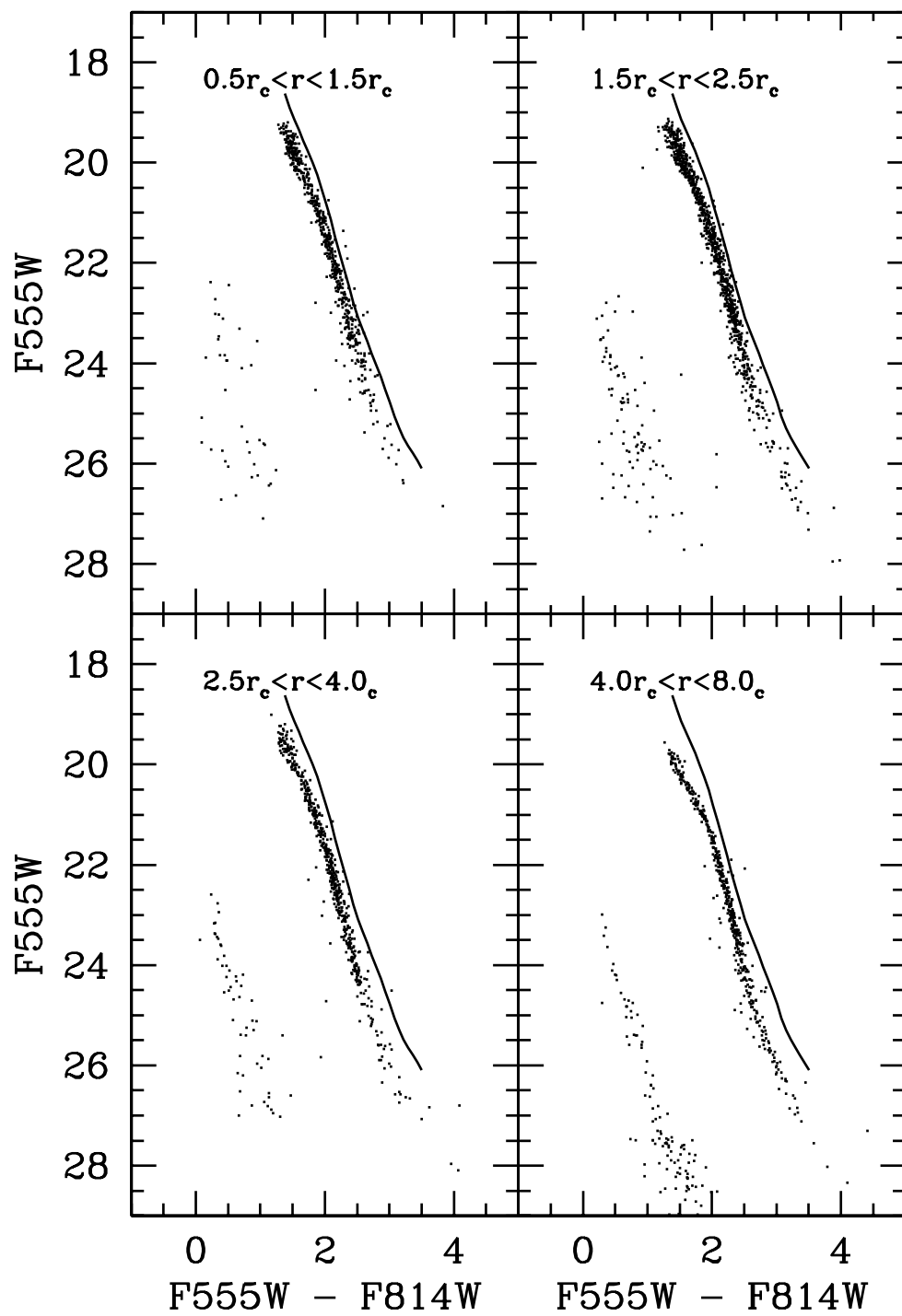


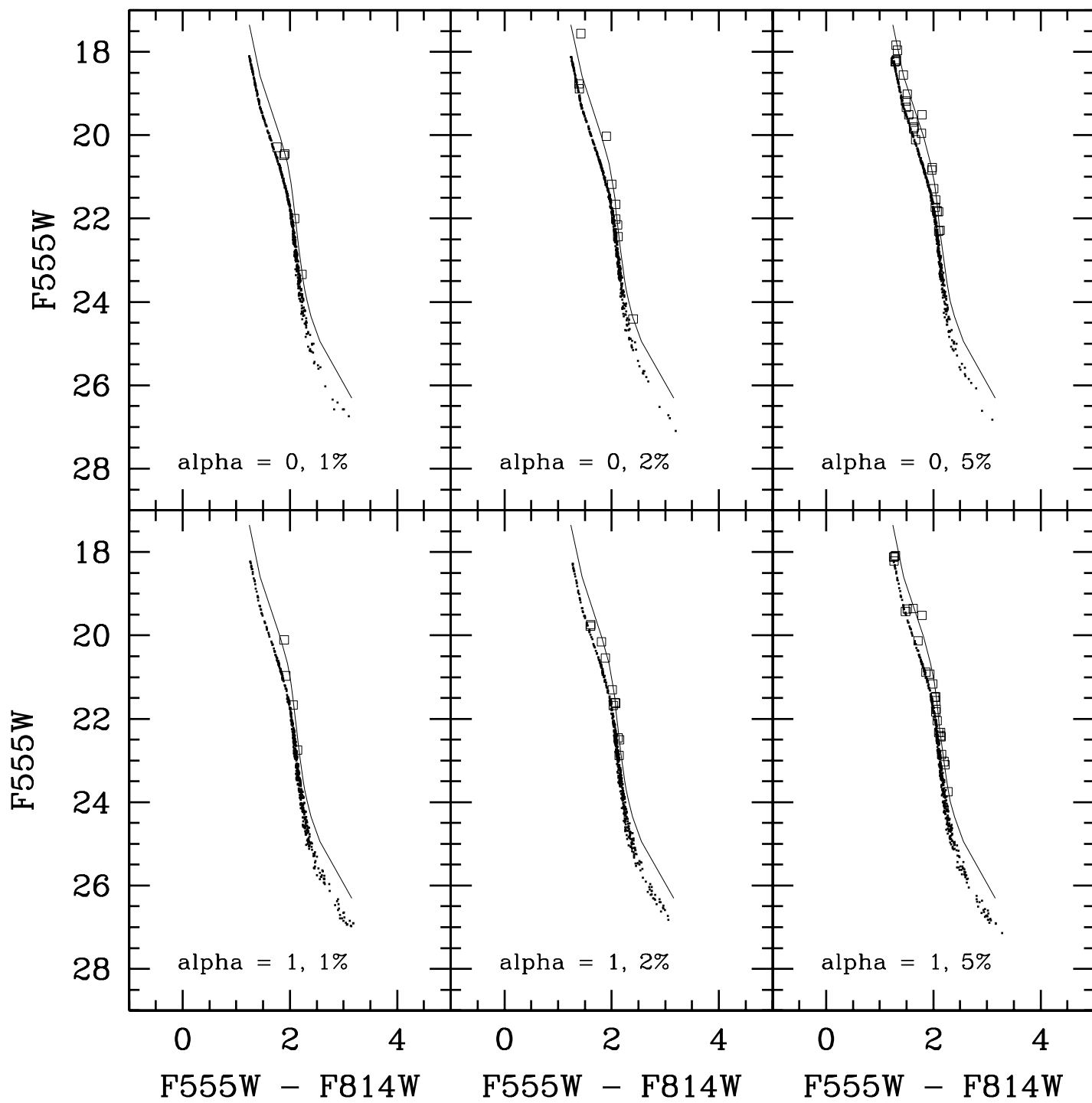


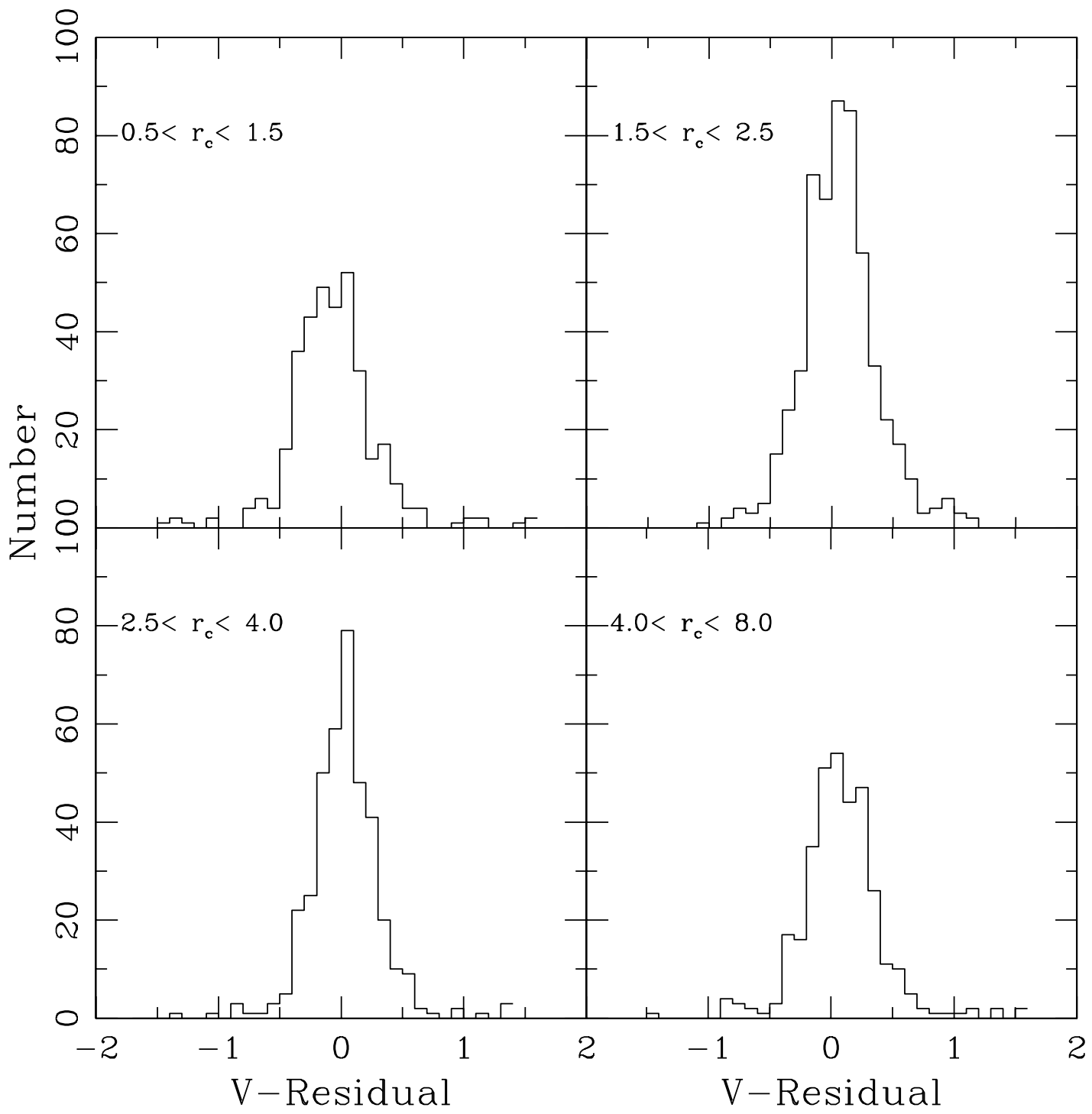


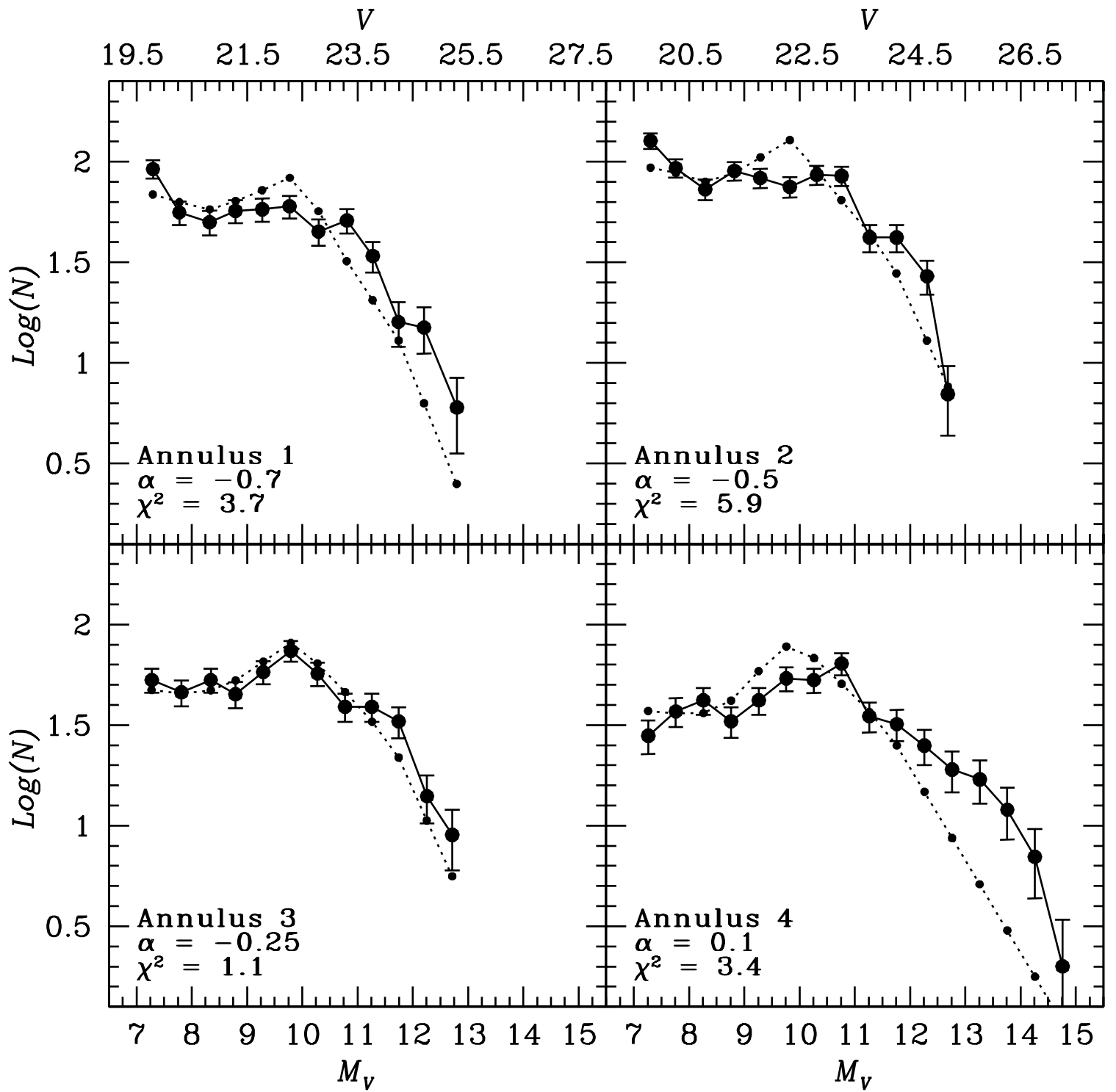


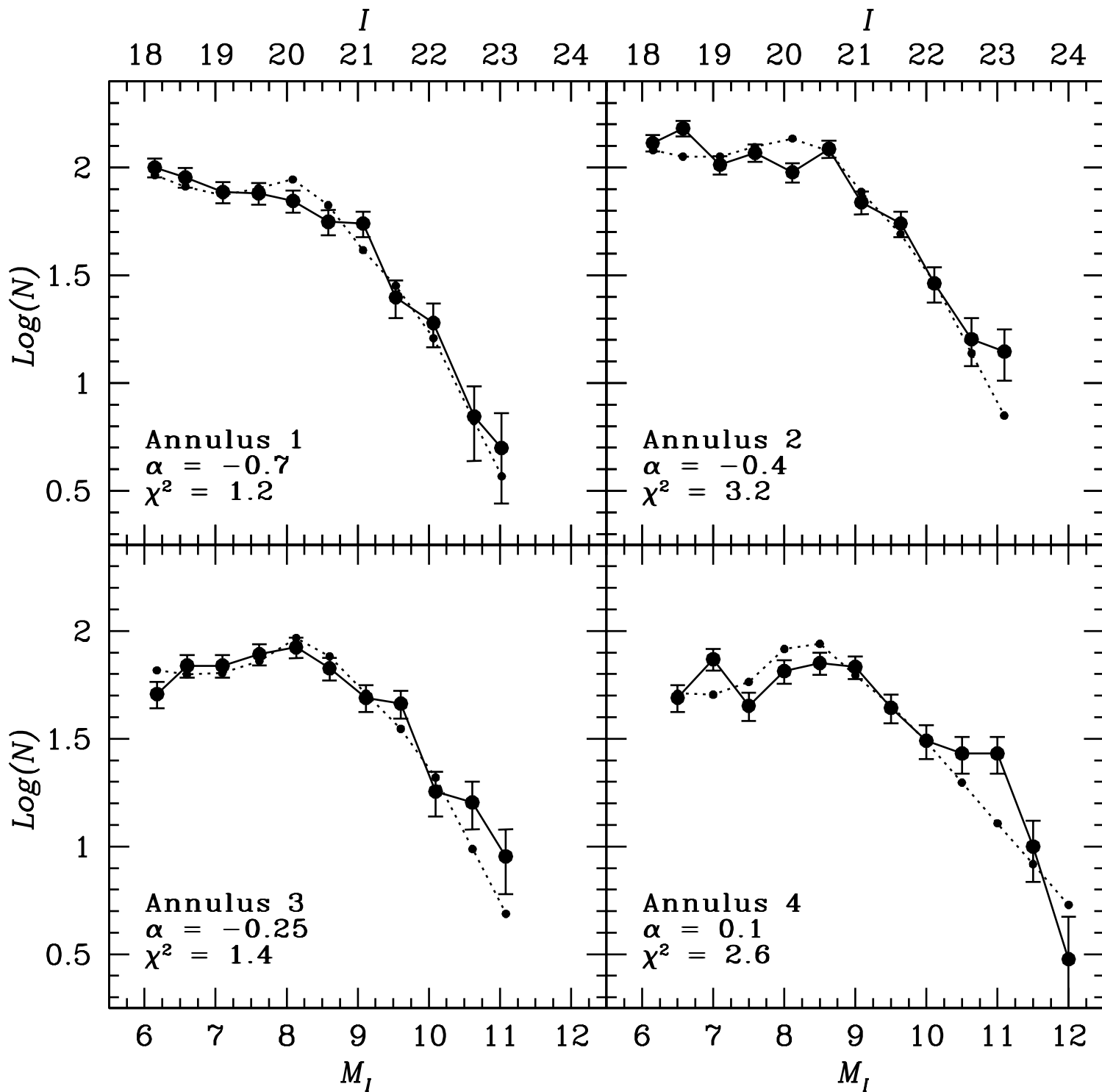












M4:SB Profile

